Tribocorrosion Behavior of Metallic Implants: A Comparative Study of CoCrMo and Ti6AL4V Under the Effect of Normal Load

by

Mihir V. Patel

Submitted in Partial Fulfillment of the Requirements

for the Degree of

Master of Science in Engineering

in the

Mechanical Engineering

Program

YOUNGSTOWN STATE UNIVERSITY

May 2019

Tribocorrosion Behavior of Metallic Implants: A Comparative Study of CoCrMo And Ti6AL4V Under the Effect of Normal Load

Mihir V. Patel

I hereby release this thesis to the public. I understand that this thesis will be made available from the Ohio LINK ETD Center and the Maag Library Circulation Desk for public access. I also authorize the University or other individuals to make copies of this thesis as needed for scholarly research.

Signature:

Mihir V. Patel, Student	Date

Approvals:

Dr. Jae Joong Ryu, Thesis Advisor	Date
Dr. C. Virgil Solomon, Committee Member	Date
Dr. Kyosung Choo, Committee Member	Date
Dr. Salvatore A. Sanders, Dean of Graduate Studies	Date

Abstract

Prosthetic implants have helped to restore mobility and increase the function of diseased joints. The modular design of joint replacement is most widely used due to the ease of anatomic customization. Modular interface such as the stem-head interface of total hip replacements is continuously subjected to wear and corrosion. CoCrMo and Ti6Al4V ELI are the most widely used metals in Total Hip Joint Replacement implant devices because of their long life, high mechanical strength, and electrochemical stability. Tribocorrosion behavior study of both metals is essential to predict the actual performance of these metals in implant and to judge which metal is better over others. The scratch test and electrochemistry of corrosion is performed on both metals to see wear behavior at varying Normal load. Three different loads were used on both metals to get a broader view. Open Circuit Potential (OCP) and Potentiostatic Polarization Resistance were measured to analyze corrosion behavior of metal along with mechanical wear by scratching the flat surface with the micromotion of the spherical ball. Potentiodynamic Polarization Resistance (PPR) were measured for corrosion behavior during an ideal condition when there is no mechanical wear. OCP measurement revealed that Ti6Al4V ELI exhibits depassivation for first few cycles of scratch but started repassivation soon with periodic depassivation. While on CoCrMo depassivation was more than repassivation resulting in continuous small drops during fretting. Ti6Al4V ELI showed better corrosion resistance at all loads during fretting. After fretting was ceased, repassivation was faster in CoCrMo than Ti6Al4V ELI. The coefficient of friction (COF) measurement during scratching is beneficial for predicting the material removal and wear debris arrest between contacting surface. PPR measurement yielded a wider range of passive zone for Ti6Al4V ELI when

swept through negative to positive voltage. Potentiostatic Polarization at three different voltage resulted in an increase in current density from baseline only in CoCrMo along with scratch at three loads. Ti6Al4V ELI was passive at all three voltage and all three loads. CoCrMo showed a higher change in current density at a higher voltage and load.

Acknowledgments

At first, I would like to give my gratitude to my advisor, Dr. Ryu. You have given me guidance and your advice have helped me a lot in the research that we started. I am thankful to you for providing your knowledge and experience through which I have gained a lot. You have given me suggestions and showed me a path for the whole bunch of questions that I have asked you. I am thankful for your patience and courage for getting me through the research. You have always helped me to the best of your ability. I would also like to thank my committee members, Dr. Solomon, and Dr. Choo. For this research, I appreciate your support, feedback, and suggestions. You both have helped me prepare for the best during the pre-thesis presentation. I would like to thank Dr. Solomon for giving me the opportunity to work with you and pursue knowledge from. You guided me whenever I asked you for any advice. I am also very much thankful to Dr. Marie who gave me the opportunity to work. The work has not only supported me financially but also given me the opportunity to increase my knowledge in a different environment. I would like to thank Dr. Byungwook Park who has imparted me knowledge on electrochemistry required for this research. I would also like to thank Prof. Viviano. Working with you is a pleasure and educational.

In addition, this research was in the flow because of my colleagues Edward Cudjoe and Yash Trivedi. You have shared your knowledge and assistance regardless when you have a busy schedule. Thank you for your presence and help when each time I needed. I would also like to thank all of my fellow researchers, past, and present for their knowledge, assistance, and support. This includes Mercedes Ferraro, Christina Seydlorsky and David Irwin.

Additional people and a team that I am thankful are Jonathan Siguenza, Jeff Tomita and Peter Vu of Nanovea Inc, Mechanical Workshop Team, Youngstown State University and the YSU Mechanical Engineering Department.

At last, I would like to thank my family members for love and support. During research work, my wife, my mother and my brother were patient enough to bear my impassive behavior sometimes. I would also like to thank my parents in law who were patient and helpful too lately. I appreciate all.

Table of Contents

List of Figures

List of Tables

Nomenclature

THJR	Total Hip Joint Replacement
MoM	Metal on Metal
MoP	Metal on Polyethylene
CoM	Ceramic on Metal
CoC	Ceramic on Ceramic
CoP	Ceramic on Polyethylene
ASTM	American Society for Testing Materials
CoCrMo	Cobalt Chromium Molybdenum
Ti6Al4V ELI	Titanium 6-Vanadium 4-Aluminum Extra Low Interstitials
UNS	Unified Numbering System
HCP	Hexagonal Closed Packed
FCC	Face Centered Cubic
FDA	Food and Drug Administration
MHRA	Modern Humanities Research Association
SCE	Standard Calomel Electrode
OCP	Open Circuit Potential
EDM	Electrical Discharge Machine
PPR	Potentiodynamic Polarization Resistance
DM	De-mineralized

PBS	Phosphate Buffer Saline
COF	Coefficient of Friction
PR	Polarization Resistance
FCP	Free Circuit Potential

Chapter 1: Introduction

1.1 Total Joint Replacement (TJR)

There are 360 joints in the human body. These joints work in relation to each other to perform daily important activities. Anatomy, branch of science concerned with the bodily structure of human beings, of joints is where the ends of two or more bones meet. Synovial joints, also known as diarthroses, are the most common and movable joints of the body. These joints contain synovial fluid. There are different types of synovial joints within the body based on the way it is attached. To illustrate the knee is a “hinge” joint due to its ability to bend like a hinged connection. The hip and shoulder are “ball and socket” joints, in which rounded end of one bone fits into a cup-shaped area of another bone. Due to many factors by injuries or disease, there can be inappropriate functioning of the damaged joint. Therefore, those malfunctioning joints in a human being would be replaced by prosthetic joints. This study is mainly concentrated on the damage mechanisms of metallic total hip joint replacement and hip resurfacing. The American Joint Replacement Registry (AJRR) 2017 data reflects 8,60,000 hip and knee replacement procedures from 4,755 surgeons at 654 institution form 2012 through 2016.

A synovial joint, which joints two bone with the fibrous joint capsule, is of ball and socket type in the hip joint [1]. It consists of an outer boundary that surrounds the bones articulating surface known as a synovial cavity. Synovial fluid is found in this cavity. Synovial membrane of this synovial joints during motion produces synovial fluid that acts as a durable layer of articular cartilage which helps in a smooth motion of the bone surfaces and femoral head in joints[2], [3]. Most body weight of the human body is share by this

hip joint along with knees during motion, standing and weight lifts. This is the main reason that hip joints and knee joints are more prone to wear and require total replacement[3]. Hip arthritis can be treated with stem cells or in the mild case with cultured stem cells procedure, but unlike other areas, it is hard to treat hip with very severe arthritis[4]. In that case, patients are pushed for Total Hip Joint Replacement (THJR).

THJR is a surgical procedure whereby the diseased cartilage and bone of the hip joint is surgically replaced with artificial materials. The normal hip joint is a ball and socket joint. The socket is a cup-shaped component of pelvis called acetabulum and the ball is head of the thighbone femur. The main components of THJR are Liner, Acetabular Shell, Femoral Head, and Stem as shown in figure 1. They are made in a combination of many biomaterials such as Metals, Ceramic, and Polyethylene. The Acetabular shell is bolted inside the hip bone. The Acetabular liner is placed in between Acetabular shell and Femoral Head. The Femoral Stem is fitted in between Femoral Head and Femur bone[5].

Many different biomaterials have been used for Total Hip replacement devices. Hip replacement devices divide into few main categories as Metal on Metal (MoM), Metal on Polyethylene (MoP), Ceramic on Metal (CoM), Ceramic on Ceramic (CoC), Ceramic on Polyethylene (CoP), etc. It is highly debatable with the superior design and combination over the other, because of patients' anatomic characteristics and daily activities. Orthopedic surgeons should be able to clearly explain why the chosen type of implant would be appropriate for individuals.

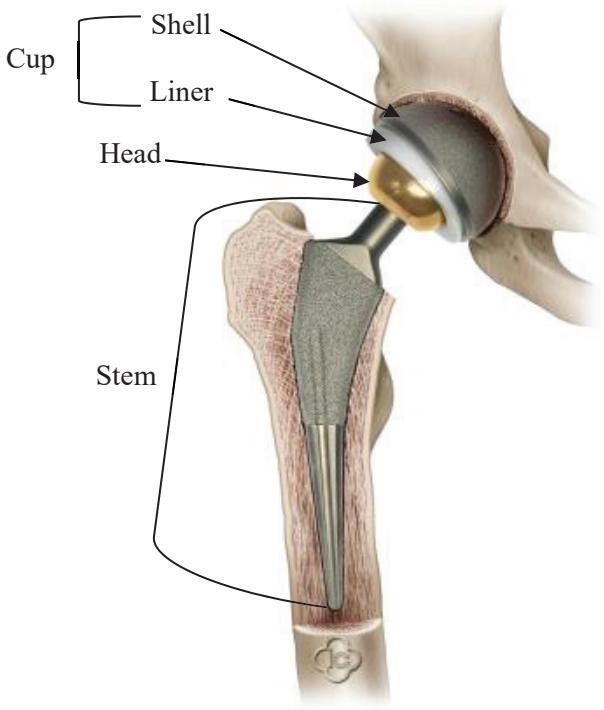

Figure 1: Main components of Hip Prosthesis

In the successful THJR surgery, the damaged surface is removed, and the prosthetic components are installed on the removed tissue to restore articular joints. The surgical procedure gets rid of the pain because the diseased cartilage and damaged bone tissue do exist. Another benefit of the replaced joint is to improve smooth articulations. The successful procedure ultimately improves quality of life. The potential risk of THJR includes infections, the adverse effect from periprosthetic tissue, and failure of the joint implant. A lifetime of THJR is about 20 in maximum, and therefore revision surgery would be required.

1.2 Biomaterials

Biomaterials play an important role in restoring function and facilitating healing for local and systemic injuries and diseases. Biomaterials may be natural or synthetic and are used to assist or replace damaged tissues. The modern biomaterials field encompasses a wide range of science and engineering in medicine, biology, physics, chemistry, and materials. Due to discoveries in tissue engineering and regenerative medicine, the field has grown significantly over the past decades. Especially, materials research has been remarkably advanced to produce medical devices and implants with enhanced biocompatibility. Metals, ceramics, plastics, glass, and even living tissue and cells can all be developed to create implantable materials. One of the important applications of biomaterial is in artificial organs and tissues, including cardiac valves, stents, and grafts; artificial joints, ligaments, and tendons; implants for hearing loss; dental implants; and nerve-stimulating devices. The common type of THJR based on the biomaterials are as below:

- Ceramic on Metal, Ceramic on Ceramic, and Ceramic on Polyethylene joints use high-density alumina and zirconia at the load bearing component in hip joints [6].
- Metal on polyethylene joint includes a plastic spacer in between two bearing surfaces to reduce friction force during articulations. recently a new plastic called cross-linked polyethylene is introduced due to their excellent strength and durability [4].

- Metal on the metal joint is a popular design of hip joints made by alloys of steel, titanium, cobalt-chromium at the variable concentrations of these metals. Metallic biomaterials widely used are summarized in Table 1.

Joint registry data suggest that newer CoC large head implant combinations might improve implant survival compared with standard implant combinations [7]. However, there was no clear evidence that affirms the newer CoC implants are superior to other MoP, small headed, and cemented implants [7]. While MoP bearings are currently the most widely used implanted prosthesis, MoM has fascinated the orthopedic society and materials science community with evident longevity of the implants. From national registry data, it has become evident since 2008 that hip replacements and resurfacing with MoM bearing surfaces have significantly higher revision rates compared to those with MoP[8]. Although approximately 1 in 5 MoP hip replacements will need revised 10-13 years after they have been implanted with higher head sizes, less than 4% of MoP implants have been revised within 10 years after insertion [9]. Furthermore, approximately 13% of hip resurfacing operations will require revision after 10 years since the primary surgery was committed[10]. With the release of this information and the subsequent recalls of the DePuy Articular Surface Replacement and Zimmer Durom hip resurfacing systems, the number of MoM hip replacements and resurfacing has reduced dramatically since 2007[9].

Table 1: Metallic Biomaterials for surgical implants and prosthesis

Titanium alloy	Cobalt alloy	Steel Alloy
TiCP-1,2,3,4	Co-28Cr-6Mo cast	Fe-18Cr-14Ni-2.5Mo
Ti-3-Al-2.5V	Co-28Cr-6Mo wrought 1,2,3	Fe-18Cr-12.5Ni-2.5Mo cast
Ti-5Al-2.5Fe	Co-19Cr-17Ni-14Fe-7Mo-1.5Mn	Fe-23Mn-21Cr-1Mo-1N
Ti-6Al-4V	Co-35 Ni-20Cr-10 Mo	Fe-21Cr-10Ni-3.5Mn-2.5Mo
Ti-6Al-4V cast	Co-20Cr-15W-10Ni-1.5Mn	
Ti-6Al-4V ELI		
Ti-6Al-7Nb		
Ti-15Mo		
Ti-45Nb		
Ti-35Nb-13Zr		

After continuous attempts to advance joint designs, the accomplishment of MoM hip resurfacing devices was reported to the orthopedic society and medical device manufacturing community. The disadvantageous results from MoM include inflammatory events in periprosthetic soft tissue and necrosis of the bony matrix. An immunological response led by wear particles and their corrosion products is likely primarily responsible for the subsequent biocompatibility problems [11]. Inflammatory pseudotumors are a major complication of failure of hip resurfacing. The clinical problems caused by a small asymptomatic lesion are followed by a massive destructive infiltrative lesion inducing loosening of implants [10]. A potential cause of hip implant failure, known as trunnionosis, mainly due to metal wear at a head-neck junction of a total hip implant. Fatigue contact

during continuous articulations at the modular tapered junction of hip implants may produce soluble and particulate debris. Migrated debris cause hip pain and adverse local tissue reactions. [9]. Osteolysis by active resorption of bone with osteoclast would be caused by synovial fluid pressure rise within the joint due to loading. This high pressure can ultimately disturb normal bone perfusion and oxygenation. Such unhealthy synovial environment results in osteocyte destruction and bone necrosis when transmitted to the membrane-bone interface [12].

Despite the above fact, MoP and MoM joint implants are prevalent joint design due to the mechanical benefits. The high strength and resistance to fracture of metals and alloys allow reliable and durable modular components in joint replacements. Also, the superior manufacturability of metals such as casting, forging and machining has fascinated the orthopedic implant industries. These advantageous mechanical properties could extend its applications to cardiovascular devices like artificial heart valves, vascular stents and neurovascular implants [13]. In addition, the good electrical conductivity of metal favors their use for neuromuscular stimulation devices. Microstructures resulted from the atomic arrangement and manufacturing processes determine mechanical and electrochemical properties. Achieved knowledge of the correlations between mechanical properties and processes are critical to achieving desired characteristics to ensure optimized performance of implants in service. High precision process and treatment of metallic hip implants used to produce smooth and hard bearing interfaces successfully reduced surface wear damages. The wear rate of MoM is estimated to be 60 times less than conventional MoP implants [14]. It is evident that MoM joints will achieve prolong longevity and delay any revision surgery. MoM hip replacements and resurfacings have traditionally been used for active

young patients. Other benefits that have observed of MoM hip arthroplasty include increased dislocation resistance associated with the large femoral head diameter and reduced osteolysis by eliminating polyethylene particles. In addition, greater bone-implant integrity of MoM hip replacements would likely improve successful of revision surgery, particularly for femoral components [8, 15].

Material's response in the human body is dependent on its mechanical properties including strength, ductility, fracture toughness and hardness[8]. The strength of material characterizes the load bearing capacity before it reaches critical damage. Yield strength and ultimate strength are used to represent the limit of stress values before the plastic deformation and maximum stress the material can withstand, respectively. The ductility of a material describes the maximum plastic strain the material can accommodate before the final fracture. The ductility of the material also influences its fracture toughness. High ductility, therefore, suggests high fatigue strength for the material when subjected to continuous cyclic loading. The hardness of a material is defined as its resistance to indentation. Hence, generally, the greater hardness would lead to higher wear resistivity [8]. Hip joints are usually subjected to a cyclic motion of multiaxial loading. Thus, in order to achieve durable joints against biomechanical loadings, it is necessary to obtain an excellent combination of strengths, ductility, and hardness for reliable prosthetic joints.

Studies on explanted joint replacements illustrated that the major causes of the implant failure are the synergistic damage from the fatigue and corrosion at the modular interface of joints. Therefore, the main purpose of this study is to evaluate the electrochemistry of corrosion along with mechanical damage under the influence of normal loads. Two major medical grade implant alloys, namely Cobalt Chromium Molybdenum

(CoCrMo) and Titanium 6-Vanadium 4-Aluminum (Ti6Al4V) are investigated. These two metals are used more often because of the superior mechanical and chemical properties as summarized below.

CoCrMo is more often used in joints due to its excellent wear and corrosion resistance properties [16]. This is obtained by the addition of carbon in the alloy which results in carbide in microstructure[17]. The higher strength of forged CoCrMo (ASTM F-799) and wrought CoCrMo (ASTM F-1537) is advantageous to produce load bearing joint components Standard chemical concentrations and mechanical properties of wrought CoCrMo are shown in Table 2. The CoCrMo matrix is an HCP phase at equilibrium. Due to the slow transformation of the phase, the matrix of both the as-cast and wrought states is mainly the meta-stable FCC phase [16].

Table 2: Chemical, Mechanical and Physical Properties of CoCrMo[16], [18]

Chemical Composition							
Chromium	Molybdenum	Nickel	Iron	Carbon	Silicon	Manganese	Cobalt
26-30 %	5-7 %	0.25% max	0.75% max	0.14% max	1 % max	1 % max	Balance
Mechanical and Physical Properties							
Tensile	Yield	Elongation	Reduction of area	Elastic Modulus	Poison's Ratio	Density	
190 ksi	135 ksi	26%	23%	35000 ksi	0.3	0.299 lb/in^3	

Ti6Al4V is used in biomedical implants due to its high strength, high melting point, biocompatibility, high stiffness to weight ratio, and corrosion resistance. Commercially pure Titanium (CP-Ti, ASTM F-67) is not strong as Titanium alloy is. The high resistance to stress corrosion cracking (SCC) of Ti6Al4V in reactive environment manifests Ti6Al4V is an obvious choice in biomedical applications. It also features good machinability. ASTM

F136 is used for wrought annealed titanium-6aluminum-4vanadium ELI (Extra Low Interstitial) alloy (R56401) in the manufacture of surgical implants. Ti6Al4V ELI alloy chemical and mechanical properties are shown in Table 3. Titanium has two main crystal structures, hexagonal closed packed (HCP) α and body-centered cubic (BCC) β. Addition of alloying elements, α phase or β phase can be stabilized, which would further change transition temperature from α to β. So it can be said that there are three categories of titanium alloys α, β, and α + β alloys[5]. For α alloy, the addition of aluminum element would stabilize the α phase. For β alloy, the addition of vanadium element would stabilize the β phase[19]. Therefore, Ti6Al4V ELI (α + β) alloy have a mixture of α and β stabilizers. The greater strength of α-phase and superior ductility of β-phase are the ideal combination for load bearing implant structure. This microstructure is capable of absorbing static and dynamic loadings that can drastically improve the longevity of implants [19].

Table 3: Chemical, Mechanical and Physical Properties of Ti6Al4V ELI**[20]**

Chemical Composition							
Aluminum	Vanadium	Carbon	Iron	Nitrogen	Hydrogen	Oxygen	Titanium
5.5-6.5%	3.5-4.5%	0.08% max	0.25% max	0.05% max	0.012% max	0.13% max	Balance
Mechanical and Physical Properties							
Tensile	Yield	Elongation	Reduction of area	Elastic Modulus	Poison's Ratio	Density	
120-125 ksi	110-115 ksi	8-10 %	15-25 %	16535 ksi	0.3	0.159 lb/in^3	

1.3 Surface Damage Mechanism

1.3.1 Wear

Soluble and particulate debris are produced due to frictional actions at interfaces during daily activities. Taking into consideration of the practical application of hip joints,

it is well known that wear is caused not only by the material properties and design but also by tribological effect [21]. Tribological conditions include surface roughness, lubrication, and kinetic forces. To understand the wear mechanism, it is necessary to correctly reproduce the tribological condition of the joint implants [22]. A close correlation between the microstructures of the alloys and the acting wear mechanisms must be understood to describe the wear behavior of joint interfaces[23]. Modifications of surface topography and wear mechanisms during tribological testing examine the lifespan of a pair of solid surfaces [24].

Multi-axial kinetic loads give rise to continuously changes in shearing modes on interacting surfaces which tends to accelerate wear rates [25]. Inertial impact during walking and running motions can attribute amplified loading up to 8 times of the body weight. Similarly, different joint motions attribute a complex mode of joint articulation. Torsional moments are also present while this movement which can be 50% higher than for walking. Ten million loading cycles simulate an implant time of 3.9 years in an active patient. For the heavyweight and very active patient, the real load conditions are more critical than those defined by the ISO standards for fatigue test. During human gait, alternate strides cause a large sliding and micro relative motion at the same time. Due to cyclic loadings during human gait and interlocked connections, the tapered interface between femoral head and stem is subjected to fretting [26]. Weighting factors of kinetic loadings due to different activities of patients are shown in Table 4. For example, a human body weight of 70-80 kg could be 5000 N force in maximum at each second step and the differential load during cycles of stride is about 4700 N [26].

Table 4: Maximum Load on the hip joint during gait

Activity	Load Multiple of body weight
Slow	4.8
Standard	4.8
Fast	7.5

There are five general processes that cause mechanical surface damage as illustrated in Figure 2. *Adhesive Wear* is produced when there is a relative load between two surfaces and one surface intrinsic material property is stronger than other. Due to continuous motion bonding and breaking of asperities occur simultaneously which tends to create wear particles[27]. Submicron wear particle is linked with accumulating plastic strain under multiaxial loading conditions up to the point where ultimate strain is reached[28]. Wear particles are released from the surface after gathering of critical plastic strain. *Abrasive wear* is produced when the hardness of the two surfaces are different. The micro-roughened hard surface plows the soft material surface leading to a large scale plastic deformation [27]. Abrasive wear results in the softer material being removed from the track which is traced by the asperity[29]. *Three-body wear* is like abrasive wear that occurs when hard particles such as metal oxide debris are embedded in a soft surface. These particles create abrasive wear removing material in the path as it acts like asperity of hard material[27]. *Fatigue wear* is produced when one surface cyclically slides the other surface that repeats shearing on both surfaces. During the continuous relative motions, dislocations are accumulated and then transferred to microcracks. Shearing mode of loads will propagate the microcracks to critical length and finally delaminate the flake-like surface layer. This process creates wear particles that can be in a range from micro to macro level in large

areas [27]. *Corrosive wear, also known as oxidative wear,* is a process in which the corrosive environment successively produces an oxide layer that is removed by frictional sliding contact. The damaged area where the protective oxide layer was removed is subjected to environmental corrosion attacks. The following asperities continually break, and the reactive environment reproduces the oxide layer. The modifications of surface properties by oxidative wear normally change wear mechanisms [27].

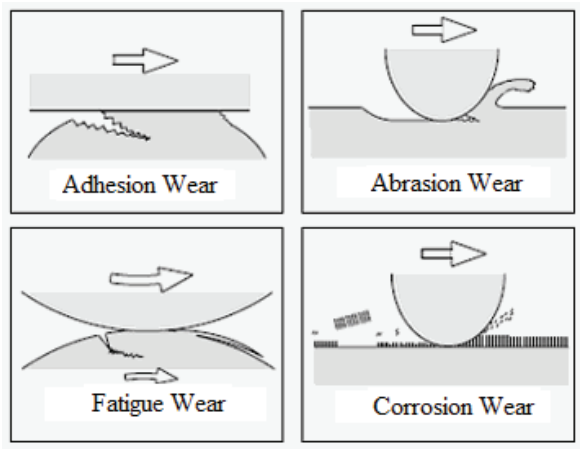

Figure 2: Schematic figure of types of wear (Modern tribology handbook, Kato and Adachi 2001)

Tribological actions of joint implants are affected by many factors including prosthetic materials, anatomic structures, physiological conditions (various protein levels), patients' lifestyles, and subsequent biomechanical loadings [30]. The resultant damage mechanism of implants is a complex blend of such causes at variable combinations. Repeated sliding contact on a small scale (fretting fatigue) in a corrosive physiological environment causes progressive damage to the metallic joint implants that limit their service life [31]. This surface fatigue damage results in the formation of soluble debris that can migrate locally or systemically. Wear debris and corrosion products may cause adverse

effects such as inflammation and necrosis in the surrounding soft tissue [31]. The debris produced by continuous sliding contact fatigue can be removed from the contact zone or on the contrary, can be entrapped between surfaces. Removed particles could be either dissolved chemically or rejected out by a hydraulic flow of the joint fluid. Wear particles undergo a large plastic strain that accelerates corrosion[26]. This hard-oxidized debris plows both contacting joint surfaces and agglomerated debris produces a complex mixture with organic matrix, known as a tribolayer. Also, contact stress generates high-stress concentrations at the wear trenches produced by wear and corrosion. These significantly large surface trenches would serve as surface cracks which are followed by stress-corrosion cracking[32].

Wear particles sizes, shapes and chemical compositions were found to influence periprosthetic tissue responses followed by subsequent complications. Such physiological sensitivity against wearing debris activates the immune system and subsequently lead to significant loss of bone [30]. Wear debris also initiates mechanical and functional instability and increases pain with a physiologic limit of joint range of motion. Unhealthy synovial environment deteriorates joint lubrication and promotes corrosion attacks. Therefore, the synergistic process results in osteolysis and hastens implant loosening and ultimate implant failure [30]. Fretting at the head-stem interface and sliding wear at the articulating surfaces of the ball and acetabular cup are two areas of concern. Fretting fatigue is surface damage process that occurs between two contacting surfaces experiencing the cyclic motion of small amplitude which is smaller than the contact area. The high contact pressure greater than hydraulic pressure of lubricant results in direct metal to metal contact. Fretting contact in the joint replacements is greatly affected by the kinetic force at the limb,

physical and chemical properties of interacting surfaces, number of cycles, and synovial lubrication.

Contact fatigue wear is characterized as progressive surface damage by continuous relative displacements exceeding dimensions of contact. In the subsequent sliding motions, the small subsurface cracks coalesce and reach critical length to propagate. Contact fatigue is a major concern at the interface leads to progressive crack propagation parallel to the interacting surface[33]. Microcracks formed during manufacturing propagates with neighboring cracks due to the shear motion of surface layers during sliding contact [33]. After the crack length reaches its critical point, delamination wear produces thin particles during subsequent continuous sliding. These trenches may serve as surface cracks which propagate during subsequent interfacial interactions. While fatigue contact, the crack propagates due to bending stress into the material and fatigue contact stress parallel to surface[33].

1.3.2 Corrosion

CoCrMo and Ti6Al4V ELI alloys are used in orthopedic implants such as screws, pins, and plates. CoCrMo forms a thin (1 - 4 nm) passive film on its surface that comprises from a mixture of cobalt, chromium and molybdenum oxides[34]. Whereas for Ti6Al4V ELI, the main reasons for their choice are the ability of the naturally formed highly stable passive oxide layer, typically 4–6 nm thick, which offers excellent corrosion protection[35]. However, this passive oxide layer possesses inferior mechanical properties. The naturally formed passive oxide layer has been found to be disrupted at very low shear stresses, even by frotting against soft tissues.

Metal ion release is also a cause of concern. Even though there is a very low wear rate ranging from 0.5 to 2.5 μm/year increased ion levels in MoM is observed as compared with other types of prosthetic devices[36]. The wear debris size ranges from particles tens of nanometers to submicron in size. Even though there is a low wear rate, the number of particles is substantial. Metal ion release can form metal-protein complexes which can lead to concerns including osteolysis, metal hypersensitivity and perivascular lymphocytic tissue responses[37]. There is rising evidence which shows wear debris and metal ions disseminate to both the surrounding tissue and bone as well as remote locations in the body, that is potential of adverse side effects[38]. Concerning this, all side effect, the use of MoM is on alert as being raised by an agency such as FDA and MHRA.

Metals and their alloys create many chemical compounds of the opposite charge in the aqueous environment which in the presence of oxygen creates a perfect environment of corrosion. The inherent human body biological and chemical conditions such as water, oxygen, protein, pH, enzymes, etc. increase aggressive corrosive environment. The electrochemical reaction between implant and body fluid interface tends to chemical consequences of oxidation and reduction[39]. The positively charged metal atoms leave the surface and mix with the liquid surrounding the implant while the dissolved oxygen in it attracts the charged metal ions and which is an anodic process.

The corrosion rate is depended upon many factors such as pH value of electrolyte, temperature, stress acting on it, the electrochemical behavior of metal, etc.[26]. Fretting and sliding wear conditions lead to fracture of the passive oxide layer. Fretting refers to friction process involving small amplitude displacements, more precisely displacements with total amplitude smaller than the contact width. Film on contacting metal surface is

subjected to fracture due to cyclic loading because of fretting and scratch[40]. Fretting corrosion is caused by the combined effect small scale cyclic wear and corrosion. The oxide layer is fractured because of this wear which exposes the reactive metal inside. This continuous process goes on resulting in the dissolution of metal ions in electrolyte and reformation of oxide layer known as repassivation as shown in figure 3. Once the oxide layer is formed corrosion ceases until next cyclic loading leads it oxide layer to fracture point. Due to the mixing of metal ions in electrolyte the chemical composition of electrolyte changes where the repassivation process occurs. The pH of the electrolyte decreases and metal ions concentration increases[34]. The oxidation and reduction process taking place may influence the biochemistry involved in biological processes. Proteins absorbed on the surface also reduce oxygen diffusion in some regions and cause preferential corrosion in those regions. Hydrogen formed by cathodic reaction acts as an inhibitor of corrosion, but the presence of bacteria appears to change this behavior and increase corrosion by absorbing the hydrogen in the vicinity of the implant[41]. The change in the chemical composition of biological media leads to a change in the composition and/or covalent structure of proteins, which can lead to the formation of antigen determinants[34]. This change in the nature of proteins, which provides a share of cell attachment of human tissue to metal surface implants, results in implants to gradually loose. This increases the further probability of fretting corrosion.

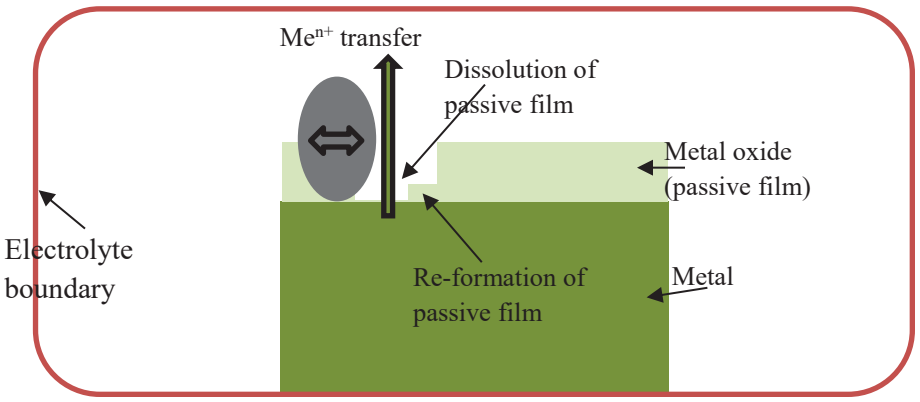

Figure 3: Fretting corrosion damage by the combined effect of oxide film fracture and metal ion dissolution

Destruction due to corrosion is a complex process. This degradation process can be explained as chemical or electrochemical damage of metal and alloys by the surrounding medium. The electrochemical properties of metal implants are defined by chemical composition, crystal structure, conductivity and galvanic effects between two contacting metals. In in vivo, there may be a combined process of metal ion dissolution and alternating oxide layer fracture and reformation, due to the simultaneous reaction of mechanical contact and electrochemical reaction.

There are few types of corrosion which can occur in the hip joint as shown in figure 4: *Localized corrosion* during which most of the metal loss occurs at non-continuous areas. In this crevice corrosion is said to be a form of pitting usually due to the localized difference in the environment[39]. *Fretting corrosion* that is caused by the vibratory relative motion of two surfaces in close contact under load. *Intergranular corrosion* at the grain boundaries in the metal structure. *Dealloying corrosion* due to the selective dissolution of one component of an alloy. *Stress corrosion cracking and fatigue* is cracking phenomenon

which includes corrosion fatigue, a mechanical phenomenon enhanced by nonspecific corrosive environments, and environmental cracking in which a brittle failure is induced in an otherwise ductile material under tensile stress in an environment specifically for the alloy system.

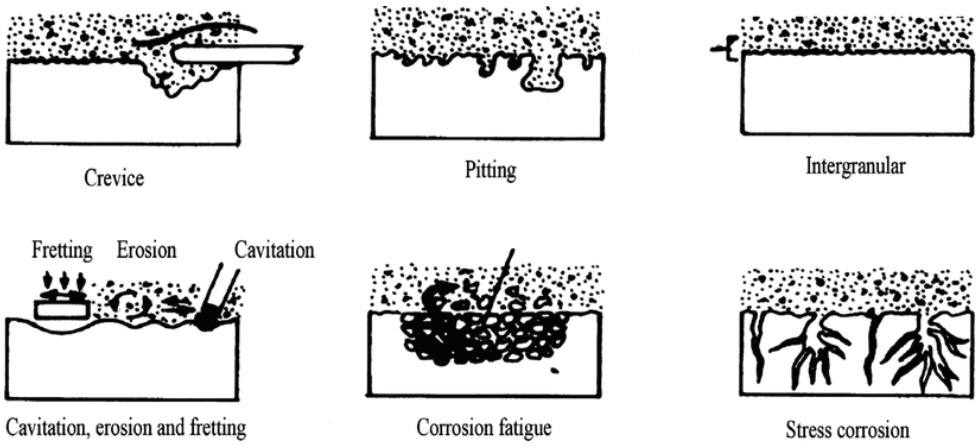

Figure 4: Different types of corrosion in the hip joint (Summary of different types of corrosion, Chaturvedi, 2009)

Fretting corrosion has been observed in bone plates and screws at the bone–stem and stem–cement interfaces of modular hip implants. Although most of the materials used are protected from environmental attack by surface oxide layers, clinical evidence for the release of metal ions from the implants has been attributed to the corrosion process[41]. It has been well accepted that the tolerable corrosion rate for metallic implant systems should be about 2.5 x 10-4mm/yr, or 0.01mils/year [19]. The repetitive loading on the implant material by human body may propagate surface cracking and lead to repetitive oxidation which leads to an increase in local hydrogen concentration by consuming oxygen in physiological body fluid and thus increasing the electrochemical reactivity. Even though new materials are continuously being developed to replace implant materials used in the

past, clinical studies show that these materials are also prone to corrosion to a certain extent [42]. Thus it can be said that two physical characteristic that ascertains corrosion in the implant are thermodynamic forces that cause corrosion due to oxidation and reduction reaction and the kinetic barrier of the surface oxide layer that prevents corrosion reactions[42].

The driving force that causes metals to corrode is a natural result of their temporary existence in metallic form. To produce metals starting from naturally occurring minerals and ores, it is necessary to provide a certain amount of energy. This energy is reverted naturally to the original state in which they were found[39]. The energy required to convert iron ore to metallic iron is returned when the iron corrodes to form the original compound. The amount of energy that required and stored in a metal or that is freed by its corrosion varies from metal to metal. The difference in energy between metals and their ores can be expressed in electrical terms that are in turn related to heats of formation of the compounds.

Metals are made up of atoms and of smaller particles which make up the atoms. These numerous particles arrange themselves in a group according to the charges they possess. Oxidation and reduction process occurs depending upon releasing and gaining of electrons respectively. Many chemical compounds split into two or more separate ions having equal and opposite charges are called ionization. It is these particles that are responsible for the conduction of electric currents[43]. All metals exhibit crystalline structure and alloys formed from these metals is greatly determined by the respective similarities between crystal lattice of these meals and by properties such as the size of the atoms. Fine-grained steel gives better strength and toughness, whereas coarse-grained steels give better machinability. Grain size has an important effect not only on physical

properties, but grain boundaries and differences in grain orientation may also result in significantly different electrochemical reactivity in metals and alloys. The pH level of electrolyte is also an important factor to further implicate corrosion behavior.

Mechanical and electrochemical properties of materials and solution are the main parameters that affect fretting corrosion behavior in hip joints. The mechanical force causes wear debris that gets gathers at the modular interface and the surrounding environment. Body tissues can respond to these wear debris and can increase corrosion which will lead to implant loosening or its failure. During fretting motion, the protective oxide layer gets a break and expose the metal inside inducing some sort of electrochemical reaction depending upon the pH value of electrolyte and amount of material exposed by trenching.

Ti6Al4V has shown very good corrosion resistance but are subjected to fretting and wear with particles of an alloy found in surrounding tissue. Galvanic coupling corrosion needs to be taken care with Ti6Al4V to avoid it particularly between pure titanium and Ti6Al4V alloy[19]. CoCrMo when studied for carbide inclusion on corrosion behavior it yielded that it did not affect corrosion mechanisms rather the presence of proteins caused dissolution thereby increasing the Cr concentration in the surrounding tissue field[44]. Studies in the laboratory on CoCrMo, when immersed in simulated body fluid, showed that cobalt dissolved from the surface and the remaining metal consisted of chromium and molybdenum oxide. There is an elevated cobalt level found in the blood due to corrosion in patients or due to the release of cobalt of the wear particles.

1.3.3 Tribocorrosion

Material stability plays a vital role in the biomedical application of metals during continuous interactions with biomedical compositions in the human body. The

electrochemical potential between any alloy and surrounding body fluid results in localized anodic reactions which further initiates surface flaws. This unwanted chemical reaction of metallic implants is further affected by mechanical loading caused during patient activities[32]. These combined effects of biochemical reactions and mechanical response result in the onset of degrading processes and results in implant failure. Previous investigation has suggested that biocompatibility problem occurs because of the high accumulation of metal ions and wear particles[32]. Toxicity due to metal produced from the concentration of these metal ions generated an awful inflammatory event in the surrounding tissue which is hard to heal.

The tribocorrosion process represents a material degradation which involves mechanical wear processes and electrochemical and/or chemical corrosion processes. The unique mechanical properties of materials are continuously modified and deteriorated by corrosion attack that progresses to premature failure of the materials[32]. Tribocorrosion has gained its importance due to the presence of the passive layer on metal that is subjected to any type of mechanical loading. Due to loading this passive layer is removed and form oxide particles which also known as debris. This debris can either be removed from the area where it is generated, or it remains there. The effect of this is different in both cases. However, the repassivation process will take place depending upon the condition of debris. The repassivation process might get delay meaning it can have prolonged corrosion or vice versa. In a passive environment, surface stress increases wear whereas in reactive environment surface stress suppresses wear during fretting corrosion. In any case, it is necessary to quantify the process of repassivation. It can be stated from the above argument that total wear (W) will not be equal to the summation of wear due to mechanical loading

(W_{ml}) without any considering corrosion and wear due to corrosion (W_{co}) without considering mechanical loading. There exist some sort of synergistic effect(W_s) between them i.e. mechanical loading will effect on corrosion and corrosion will have some effect on mechanical loading[45]. Therefore, wear can be explained as below by simple equation.

$$W=W_{ml} + W_{co} + W_s$$

Tribocorrosion is a very complex phenomenon. Many factors can affect or can shape the wear. For example, the crack starts propagating under reciprocating sliding conditions at fretting even after only a small number of contact events. Another parameter is stirring of the corrosive environment along the surfaces of the contacting part caused by their relative moment[45]. It affects tribocorrosion because such a stirring alters the transport kinetics of chemical species produced near the surfaces due to corrosion-related reactions[45]. Thus, it is important to keep many factors to be kept in mind of which some of them listed below while studying tribocorrosion.

- The debris can accelerate or reduce wear compared to the environment where debris does not exist, e.g. polarized in sliding contacts with great cathodic potential[45],
- Galvanic coupling between worn and unworn areas is established. It accelerates anodic dissolution in the area of depassivation of metal[45],
- The galvanic coupling may occur in between to contacting material[45].
- Accumulation of dissolved species may occur in the contact surrounding liquid. This can make the medium more aggressive chemically or electrochemically[45].
- Mechanical loading in the contact area and its nearby zone may cause a work hardening of the materials. This work hardening can alter the kinetics of corrosion and/or repassivation processes[45].

The formalism of tribocorrosion originally proposed (Watson et al., 1995) describes further clarity to the above equation. The electrochemical mass loss due to corrosion during scratch is expressed by $C=C_0$ (mass loss without sliding with same test condition) + C_M, where C_M is the amount of corrosion induced by wear[45]. The total mass loss, W, can be determined at the end of a scratch test by 3D scan profilometer. That total mass loss can be compared to the electrochemical mass loss under sliding, C, from the equation: W = C + M in which M is the mechanical mass loss. This mechanical mass loss can also be expressed by $M = M_0 + M_C$, where M_C is the excess mechanical mass loss due to corrosion[45]. This formalism now allows a general definition of the synergy, S, between corrosion and mechanical processes in case of tribocorrosion as:

$$W = C_0 + M_0 + S, \text{ where } S = C_M + M_C$$

The cyclic sliding results in repetitive stress variation from compressive to tensile at the crack tip[33]. The magnitude of it is dependent on the normal loading and kinetic friction coefficient. The combined effect of plastic surface deformation, the nature of oxide film and mechanically stimulated corrosion that results in wear debris. The in vivo tribological aspects of hip replacements are highly variable and depend on different conditions inherent in the patients. Therefore, it is hard to simulate all involved conditions in a laboratory by a single standard pre-clinical test. There is an unstable oxide film growth which will significantly modify the physical and mechanical properties of the metal surface and corrupt the wear resistance. Hence, they are prone to crevice corrosion.

Surface degradation can be caused by either mechanical simulation or corrosion and is followed by other[33]. After initial surface damage, the anodic process subsequently continuous corrosion attack and stress corrosion at pit increase damage. The oxide layer

will try to protect corrosion. The optimized oxide film thickness will try to improve wear resistance as well as reduce the friction coefficient.

The overall phenomenon of tribocorrosion can be seen in figure 5. The mechanical loading and sliding causes wear debris. Due to the removal of oxide layers and surrounding liquid coming in contact with metal surface cause oxidation.

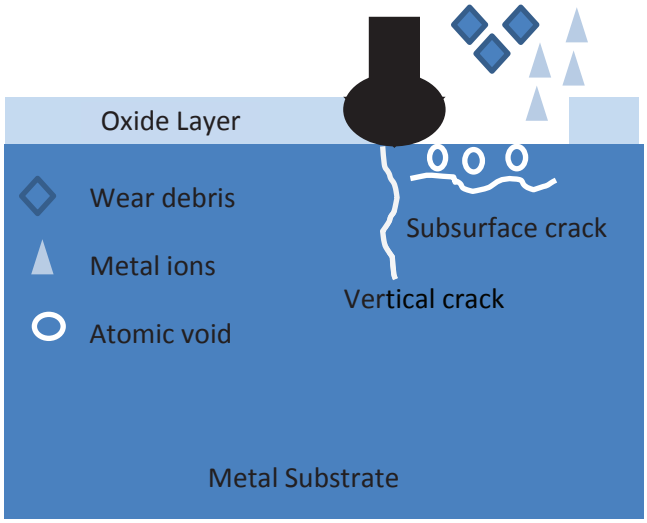

Figure 5: Tribocorrosion process in the metal substrate

1.4 Research Objectives

CoCrMo and Ti6AlV4 ELI are two crucial metals that are used in hip joint implants. They have manifested their long useful life due to superior mechanical strengths and electrochemical stability during active articulations in the human body. Previous studies were done on the above metals independently and in vitro simulations of tribocorrosion presented contrary results. CoCrMo implant surface showed a higher wear rate than the Ti6Al4V implant surface despite the higher hardness of CoCrMO than Ti6Al4V. Corrosion and wear and more broadly speaking tribocorrosion behavior of these two metals remain a concern and has been found to be significantly limit the useful life of the implants. This

study will help predict the overall life cycle of metallic orthopedic implants under fatigue loadings at the modular joint replacements for the vast application for biomedical devices. It will also help to understand the tribocorrosion behavior of these two metals to compare and understand the complicated process of the alloys.

The experimental setup is customarily designed to mitigate the functional requirement of studying tribocorrosion behavior of two metals. Three different loads 50 mN, 100 mN, and 200 mN which sweep the range of average pressure acting on a hip joint is therefore studied to see the variation of tribocorrosion in these two metals. For that various machines are used to simulate the in-vivo condition in the hip joint. A reciprocating different three loads with small frequency are applied on the metals in the present of simulating fluid namely Phosphate Buffer Saline (PBS) to study wear due to electrochemical corrosion and mechanical corrosion along with their synergistic effect. Open Circuit Potential measurement, frictional force and coefficient of friction measurement, Potentiostatic and Potentiodynamic polarization resistance measurement are done to observe and compare their effect on two metals.

1.5 Thesis Outline

This paper starts with outlining the necessary background information. Chapter 1 covers a range of topics from Total hip joint Replacement, Biomaterials, Surface Damage Mechanism. These topics further explain about modern hip implants, various biomaterials, and their significance. It also explains the surface damage such as mechanical wear, corrosion, and tribocorrosion which combines tribology and electrochemical corrosion effect on hip joints.

The investigation of two metals based on three normal loads is explained in Chapter 2 through Chapter 4. Chapter 2 provides information on Characterization methods in which how the surface damages are taken into consideration and investigated with the specific method to know the behavior of that damage in in-vivo condition and replicate in this investigation. It also explains briefly about the materials and experimental method used to approach this investigation. Chapter 3 describes results and a brief discussion of various methods used such as Open Circuit Potential measurement, Potentiodynamic measurement, and Potentiostatic scan.

The paper ends with Chapter 4 which provides the overall conclusion and future work that could be done to further clarify the results of this study.

Chapter 2: Methods

2.1 Characterization methods

2.1.1 Wear

Wear resistance is an important factor which determines the longevity of the component in mechanical systems. Surface layer coated on the element at the tribological interface is a common technology to reduce friction and wear. The main aim of coating is to provide smoothness and hardness to the surface resulting in less frictional forces during the operations. Reduction of the friction is important and dependent upon the tribological conditions of the component and the counter surface material used. Moreover, mechanical and microstructural characteristics are also important to achieve higher strength and hardness that directly promote greater wear resistance [46].

The reciprocating wear scratch test was performed on Ti6Al4V and CoCrMo to replicate cyclic sliding contact fatigue that simulates repeated articulations in a hip prosthesis during daily motions. A nanoindenter based mechanical tester (Nanovea, Irvine, CA) was utilized for the fretting fatigue contact experiment. The mechanical tester consists of a micro newton scale load cell and nanometer scale depth sensor with a high-resolution step-motor motion stage. The nano-resolution (nN) load cell monitors precise normal loads and the piezoelectric feedback module measures the displacement responses. The high-resolution motion stage accurately controls the lateral motion of the specimen relative to vertical spherical slider motions. The indenter used to perform reciprocating sliding was a 3mm spherical ball made from Aluminum silica ceramic. The ceramic slider head was mounted to a customized and assembled to create a non-conducting slider material. This

sliding contact test between a ceramic head and a specimen surface was performed to simulate fatigue contact at the modular interface of prosthesis wherein femoral head contact on a femoral stem as illustrated in Figure 6. The wear test was conducted in a phosphate buffer saline solution to simulate the corrosive body fluid environment effectively.

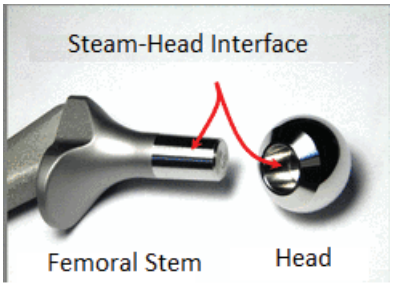

Figure 6: Stem head interface in hip joint

Hertzian contact pressure theory was used to evaluate the elastic normal loads. Elastic limit was estimated to determine the range of varying normal load to apply elastic contact pressure and semi contact radius. Using elastic modulus and poison's ratio of Aluminum Silica ceramic ball and both metals, the composite elastic modulus is calculated as below:

Composite Elastic Modulus Calculation(E_r):

$$\frac{1}{E_r} = \frac{1 - {v_1}^2}{E_1} + \frac{1 - {v_2}^2}{E_2}$$

Here subscript 1 *is CoCrMo or Ti6Al4V ELI and* 2 *is Aluminum Silica ceramic balls.*

For CoCrMo

$$\frac{1}{E_r} = \frac{1 - 0.3^2}{241} + \frac{1 - 0.21^2}{310}$$

$\therefore\ E_{r_{CoCrMo}} = 143631\ MPa$

For Ti6AlV4 ELI

$$\frac{1}{E_r} = \frac{1-0.3^2}{114} + \frac{1-0.21^2}{300}$$

$\therefore\ E_{r_{Ti6Al4V}} = 89535.2\ MPa$

After calculating composite elastic modulus semi-contact radius is calculated by using formulae as shown below. Using that Average contact Pressure and % of Yield Stress used is calculated. From this calculation, it can be found that even going to the maximum load that machine can apply metal in stress is still in the elastic region. Results of this calculation are shown in table 5 and table 6 for CoCrMo and Ti6AlV4 ELI respectively.

$$Semi-contact\ Radius\ (a) = \left(\frac{3WR}{4E_r}\right)^{\frac{1}{3}};\ Here\ R\ is\ radius\ of\ sphere = 1.5\ mm$$

$$Average\ contact\ Pressure\ (P_r) = \frac{3W}{2\pi a^2}$$

$$\%\ of\ yield\ stress = \frac{\frac{W}{\pi a^2}}{\sigma_{yield}}\ x\ 100$$

Table 5: % of Yield stress due to varying load for CoCrMo

Load 'W' (N)	Semi-contact radius 'a' (mm)	Average contact Pressure 'Pr' (Mpa)	% of Yield Stress
0.05	0.0073	446.1	31.97%
0.1	0.0092	561.9	40.29%
0.2	0.0116	708.1	50.76%

Table 6: % of Yield stress due to varying load for Ti6Al4V ELI

Load 'W' (N)	Semi-contact radius 'a' (mm)	Average contact Pressure 'Pr' (Mpa)	% of Yield Stress
0.05	0.0086	325.5	28.63%
0.1	0.0107	410.1	36.07%
0.2	0.0136	516.7	45.44%

The reciprocating wear test parameters are selected given the oscillating frequency of 1 Hertz of travel in a normal walking motion. The in-vitro fretting fatigue test is carried out for a time period of 60 minutes that correspond to 1800 cycles of reciprocations. The slider speed of 12 mm per minute is applied with a scratch length of 200 μm. The test parameter for the reciprocating wear test is summarized in Table 7. The normal force and indenter penetration depth were continuously monitored during the test in ambient conditions with controlled humidity (35±3%) and PBS solution. The wear test is repeated three times for each load on the specimen with the consistent testing parameters and environments.

Table 7: Wear Testing Parameters

Testing parameters	Values
Type of test	Reciprocating
Varying Load (mN)	50, 100 and 200
Scratch length	200 μm/100 μm
Scratch speed	12 mm/min
Metal	CoCrMo/ Ti6AlV4 ELI
Wet condition media	PBS

The tested areas are inspected using an optical microscope to investigate the size and shape of wear trenches. This observation will also help examine the mechanisms of wear and corrosion or any debris developed. These inspections are compared for two metals at different forces.

Sliding contact motion during monitoring potentiostatic polarization responses are done in the length of 100 μm. Other parameters in this test are the same as shown in Table 7.

The frictional force (F) is measured and converted to a coefficient of friction (COF) during the course of fretting contact tests. The result will assist to understand the surface damage process on two specimen surfaces.

2.1.2 Electrochemistry

Many corrosion phenomena can be explained in terms of electrochemical reactions. Measurement of current-potential relations under carefully controlled conditions can yield information on anodic and cathodic behaviors and further corrosion and passivation of the material surface in the surrounded environment. When a metal is exposed to a corrosive medium, both oxidation and reduction processes occur on its surface. Generally, the metal oxidizes, and the solvent is reduced. The metal must function as both anode and cathode, and both anodic and cathodic current occur on the specimen surface. Any corrosion processes that occur are generally a result of anodic currents.

OCP measurement:

Three electrode method is used to connect potentiostat to an electrochemical cell. Potentiostat depending on the electrolyte ionization will measure current and voltage in that. The cleaned CoCrMo/Ti6Al4V ELI acting as the working electrode, while a saturated calomel electrode (SCE) and a titanium wire served as the reference and cathodic electrodes, respectively is connected to a potentiostat. These electrodes along with metal embedded in epoxy are placed in a customized stage where fretting/sliding contact corrosion is measured when exposing to the electrolyte solution. A ball-on-flat contact

configuration that involves Ø3 mm alumina-silica ceramic ball moving against stationary CoCrMo/Ti6Al4V ELI was chosen so that large contact stresses could be achieved under low loads. The arrangement was done in such a way that alumina-silica ceramic ball (part of the whole indenter) and metal are totally immersed in the electrolyte solution. The metal was kept in the electrolyte solution for 60 minutes and allowed to stabilize before performing any corrosion experiment. The fretting/sliding contact corrosion test arrangement was connected to a potentiostat to track the response of metal in the electrolyte. The open circuit potential (OCP) measurement was run to check corrosion and no additional potential are added by potentiostat at first. The change in OCP is measured as a function of time to evaluate the performance of both alloys under fretting/sliding contact conditions for one time in wet condition with PBS as electrolyte with scratch and in wet condition with PBS as electrolyte without a scratch. The corrosion tests were repeated at least two times to verify the reproducibility of the test results.

The change in potential in the OCP measurement test reveals the type of reaction, i.e. anodic or cathodic, occurring at the metal surface depending on the passive surface layer. If there is an adsorption thickening of passive film or repassivation of the oxide layer on the metal, the potential will increase along with time meaning anodic reaction is taking place v/s reference electrode [35]. Whereas the decrease in potential along with the time of metal v/s reference electrode is suggestive of the protective layer being damaged and the material beneath it which is reactive is exposed and electrochemical reaction starts in which metal dissolution occurs which suggest the corrosion of metal[34], [35]. This electrochemistry of corrosion depends on many factors such as chemical nature of the electrolyte, amount of load, amount of friction during load application, the thickness of the

passive layer, repassivation process inherent in the metal, etc. [34], [35], [47]. However, open circuit potential measurements provide limited information on the kinetics and mechanism of surface reactions occurring on the material. The open circuit potential recorded during bi-directional friction tests in which working electrode is moved against the loaded indenter is considered to be a mixed potential reflecting the combined state of the unaffected material surface and the material from the wear track. A galvanic coupling between rubbed and unrubbed parts on the layer surface may take place. The measure open circuit potential is then an average value depending on current density distribution over the whole layer surface exposed to a corrosive environment[46].

Polarization Resistance Technique:

CoCrMo and Ti6Al4V ELI in some specific environments lose their inherently chemical reactivity and become very inert. They create barriers, very thin oxide films, on exposed surfaces between the environments and the metals resulting in much higher corrosion resistance. This phenomenon is called passivity. However, in some circumstances, the passive film can be destroyed and thus it makes the same metal active. Also, the morphology, thickness, and chemistry of oxides change in solution and depend on the surface potential and solution chemistry. Such a change could cause a skip in corrosion rate to several thousand times. Previous studies have explained that for CoCrMo oxide only forms at electrode potentials more than -500 mV (vs Ag/AgCl) in PBS[48]. The thickness increases almost linearly with potential from 2.2 nm at -0.35 V (vs Ag/AgCl) to 3.1 nm at 0.25 V (vs Ag/AgCl)[48]. At lower potentials, the passive oxide is mainly Cr_2O_3. The polarization technique is a method for investigation of such and similar behaviors of various metals with their environments.

When a metal is in contact with a corrosive liquid and specimen is not connected to any instrument the metal assumes a potential, relative to the reference electrode, and is known as corrosion potential, E_{corr}[42]. Also, these currents are exactly equal in magnitude so there is no net current to be measured. E_{corr} can be defined as the potential at which the rate of oxidation is exactly equal to the rate of reduction. The metal is at equilibrium with the environment even though it might look that it is corroding. It is important to stress that when a specimen is at E_{corr} both polarities of current are present. If the metal is polarized slightly more positive than E_{corr} then the anodic current predominates at the expense of the cathodic current[39]. As it is driven further positive the cathodic current part becomes negligible when compared with anodic part and vice versa.

Each Metal has a tendency to dissolute in the liquid surface as most of the metals do not possess an oxide layer. Metals such as Ti6Al4V ELI and CoCrMo have reasonable oxide layer. Due to this oxide layer, it will try not to dissolve in liquid. If some voltage is applied to the system, it will react and the oxide layer depending upon the voltage will passivate or depassivate. It is important to know this tendency of a metal to understand its corrosion process. A mostly negative voltage of some values will act as passivation support. But after some point, it will depassivate even without scratching. The tendency to resist this corrosion is called polarization resistance. Polarization Resistance depends on the amount and quality of the oxide layer present on the metal substrate. Two types of Polarization Resistance technique will be used:

Potentiodynamic Polarization Resistance (PPR) test is performed on the metal surface to measure the corrosion rate without fretting. Human being while sitting and sleeping does not apply load on joints. Corrosion process is still going on due to

inflammatory body fluid. To simulate that PPR test is done. In this test, the potential is varied at a very small rate and current density is measured throughout that range.

Potentiostatic Polarization test was performed to see corrosion behavior at constant voltage when fretting is initiate. A voltage was applied to the system and current density was measured with respect to time. The change in current density will indicate the passivation and depassivation process.

2.2 Materials and preparations

Both metal alloys CoCrMo and Ti6AlV4 were manufactured to a size of W1.00 mm x H2.54 mm x L22.95 mm using Electrical Discharge Machining (EDM). EDM was used to minimize residual stress and cut into precise dimensions without changing chemical and physical property. The manufactured specimens were embedded in epoxy for ease of surface finishing and mounting in the experiments as shown in Figure 7. The exposed area then becomes 0.0254 cm^2

Specimen were embedded in epoxy, both metals were mechanically polished using various grades of SiC paper (600 grit size, 1000 grit size and final with 1200 grit size). This was followed by rubbing of Ti6AlV4 ELI with Colloidal Silica on Chemomat Polishing cloth for 10 to 15 minutes until it has mirror-like finish (Ra = 0.02_m). It was then rinsed with demineralized (DM) water. Similarly, CoCrMo is rubbed with Alumina-0.05 μm on Ultrapad Polishing cloth for 10 to 15 minutes until it has mirror-like finish (Ra = 0.02_m). It was then rinsed with DM water. After that, both metals are sonicated in acetone, methanol and DM water consecutively for 180 seconds.

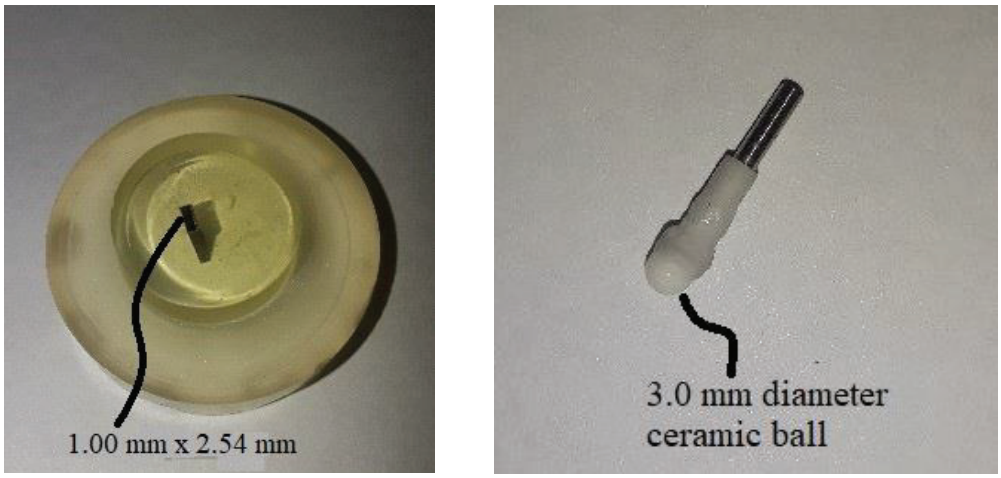

(a) (b)

Figure 7: (a) Metal embedded in epoxy. (b) Customized Indenter

While conducting the tribocorrosion study, the nonconductive ceramic slider is used inside the electrolyte to observe electrochemical response only from the specimen surface during the interactions. A 303 stainless steel rod of size 1.5875 mm diameter is used that fits in the load cell of the nanoindentation module. On one end of this rod, 3 mm aluminum silica ceramic ball and alumina tube are attached to securely separate the steel rod from the surrounding electrolyte. The ceramic ball is carefully sonicated in acetone, methanol and distilled water for 180 seconds before each test.

Custom design of the liquid cell to perform the electrochemical test is prepared taking into consideration space, the nano tester can accommodate and access to electrochemical elements including a reference electrode and the counter electrode. The bottom surface of the sample that corresponds to the working electrode is in contact with aluminum foil to electrically connect to the potentiostat controller and securely prevent from leakage of the electrolyte. The 3D views of the stage are shown in Figure 8. The stage is made up of three parts: a. Top Part made up of Nylon b. Middle part made up of Nylon

c. Bottom part made up of steel (Dimensions same as part ‘b’). All these three parts are connected with bolts and nuts sandwiching sample, using a nitrile ‘o’ ring to stop electrolyte passing from the top part of the stage to middle part. This state is washed completely before each use and air dried.

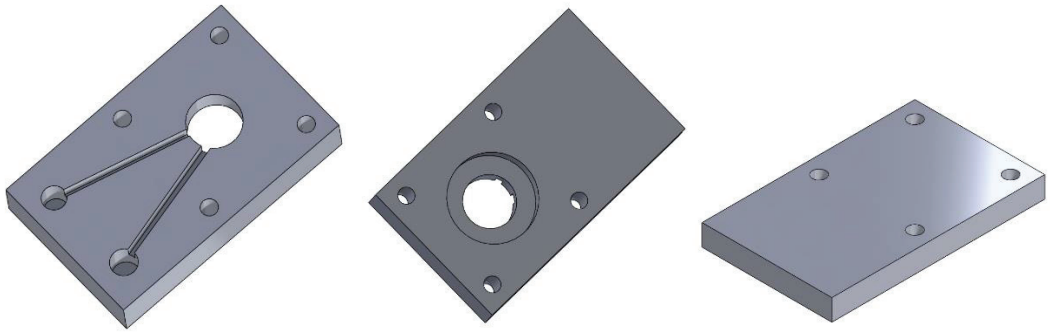

(a) (b) (c)

Figure 8: Stage parts (a) Top view of top part (b) Bottom view of top part (c) Middle part

Phosphate Buffer Saline (PBS) is used as an electrolyte as PBS is a simulate fluid for body fluid. As per ASTM F2129-2003, PBS was specified as a standard solution for testing[49]. It is frequently used in biological applications as it closely mimics the pH, osmolarity and ion concentrations of the human body. Though other solution can be used depending on the application but for this study PBS is used. The electrochemical test setup is integrated with the instrumented friction table that can monitor friction forces during sliding contact. The integrated mechanic-electrochemical setup is mounted on the nano tester machine to perform a mechanical-chemical test.

All tribocorrosion tests are performed in liquid at the temperature 26.6ºC. The representative schematic of the final design of the tribocorrosion apparatus and wiring are shown in Figure 9. The specimen and liquid are connected to potentiostat controller

(Gamry Instruments, PA) through a calomel reference electrodes and a 0.9 mm diameter platinum counter electrode.

2.3 Experimental Process

The cleaned sample (Ti6AlV4 ELI or CoCrMo) is mounted in the liquid cell. The space above the sample in the stage is filled with PBS solution which acts as an electrolyte. As illustrated in Figure 9, the specimen and liquid are connected to the potentiostat controller through a calomel reference electrodes and a 0.9 mm diameter platinum counter electrode. The potentiostat is connected to a computer to monitor open circuit potential (OCP) and polarization resistance (PR). The stage is placed under the slider head mounted on nano tester machine. The spherical slider is lowered to touch the sample and apply the desired normal load at the rate of transverse motion of the specimen.

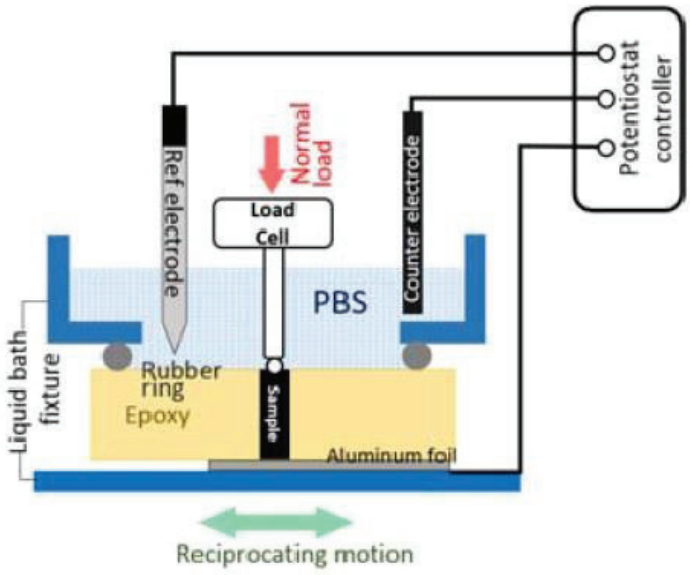

Figure 9: Test arrangement

OCP measurement:

For OCP measurements for both Ti6AlV4 ELI and CoCrMo metals, a potentiostat is operated to monitor potential changes for 60 minutes as dwell time (without sliding) to stabilize the system and to ensure the system has reached its steady state. A system is said to be stabilized if potential does not change at the rate of less than 1 mV/min. As per new inclusion in ASTM F2129 in 2006 if a change in potential is less than 3 mV/min than the system is considered to be at equilibrium. After 60 minutes dwell period, sliding motion is started with the parameters set as described above. This fatigue contact test is continued for 60 minutes. Coefficients of friction also are measured simultaneously throughout the sliding contact tests. After sliding contact is ceased, the potential is measured for 30 minutes to observe the recovery of the damaged oxide surface. The test is repeated 3 times to show the repeatability of the experimental results. The values of OCP measurement are analyzed and compared with other metals at the same load.

PPR measurement:

In this test voltage is varied with respect to reference electrode from -1.0 V to +1.5 V with a scan rate of 0.167 mV/s. These parameters were used in many research papers on other metals to see distinct zones on plots. The change in current density with a change in voltage is measured. Results were measured and discussed in the result section to see all the zones and corrosion rate.

Potentiostatic Polarization measurement:

In this test, three constant voltage -0.5 V, 0 V and +0.5 V each is applied for 3600 seconds on the system. With each voltage-current density is measured and plotted against

time. For the first 600 seconds, the system is allowed to stabilize. After that fretting is started as discussed in section 2.1.1. Once the fretting is completed the system gets stabilize for another 900 seconds. Here the increase in current density will suggest depassivation and decrease in current density is repassivation. Passivation, Depassivation, and Repassivation are observed and discussed in the result section.

Chapter 3: Results and Discussion

3.1 OCP measurement:

Open circuit potential results measured during cyclic sliding contacts on both CoCrMo and Ti6Al4V surfaces using a calomel reference electrode are summarized as a function of normal loads in PBS solution. The average potential drops were compared with different normal loads to determine the electrochemical stability during active mechanical stimuli. It illustrated that when a protective passive film is damaged the potential drops to the negative values with a consequent increase in anodic current. [50]. The evolution of the potential during continuous sliding would explain the oxidation chemistry of titanium and chromium against wear and corrosion.

3.1.1 For Normal Force 50 mN:

The change in potential was measured with a normal load of 50 mN (other parameters same as shown in experimental methodology) before the fretting was initiated (dwell), during fretting (active articulations) and after fretting motion was ceased (recovery) on CoCrMo and Ti6Al4V ELI as shown in Figures 10-12. The potential was monitored until stabilized. After 1 hour dwell period, the reciprocating motion of the spherical slider was applied at 50 mN of the normal load. There is a significant potential drop on the CoCrMo surface due to the exposure of metal through a damaged oxide layer to a PBS solution. However, the potential drop on the Ti6Al4V surface is insignificant as illustrated in Figure 11. The average potential drop by fretting contact compared in Figure 12. It is evident that the potential of Ti6Al4V ELI instantaneously drops as soon as the slider motion is initiated but spontaneous repassivation takes place and the potential is gradually recovered to its original potential of dwell period while the fretting motion of the slider is

continued. It is notable that the presence of the electrolyte beneficial for titanium to reform the stable oxide layer. Whereas the fretting wear on CoCrMo continually drops the potential until the sliding motion is ceased. It illustrates that the mechanical strength of the reformed chromium oxide layer may not strong as the original passive layer formed in ambient. During fretting on CoCrMo surface, rapid fluctuation in potential illustrates repetition of breakage-reformation of the oxide layer in PBS[50]. A small potential drop of Ti6Al4V at 50 mN describes the minimum pressure to activate electrochemical reaction is approximately 325 MPa, corresponding to 28% of the yield strength of Ti6Al4V. After fretting stops, CoCrMo surface is rapidly repassivated while Ti6Al4V was readily repassivated during fretting motion. Therefore, the Ti6Al4V presented desirable oxide chemistry that recovers the damaged surface by mechanical stimuli at 50 mN normal loads.

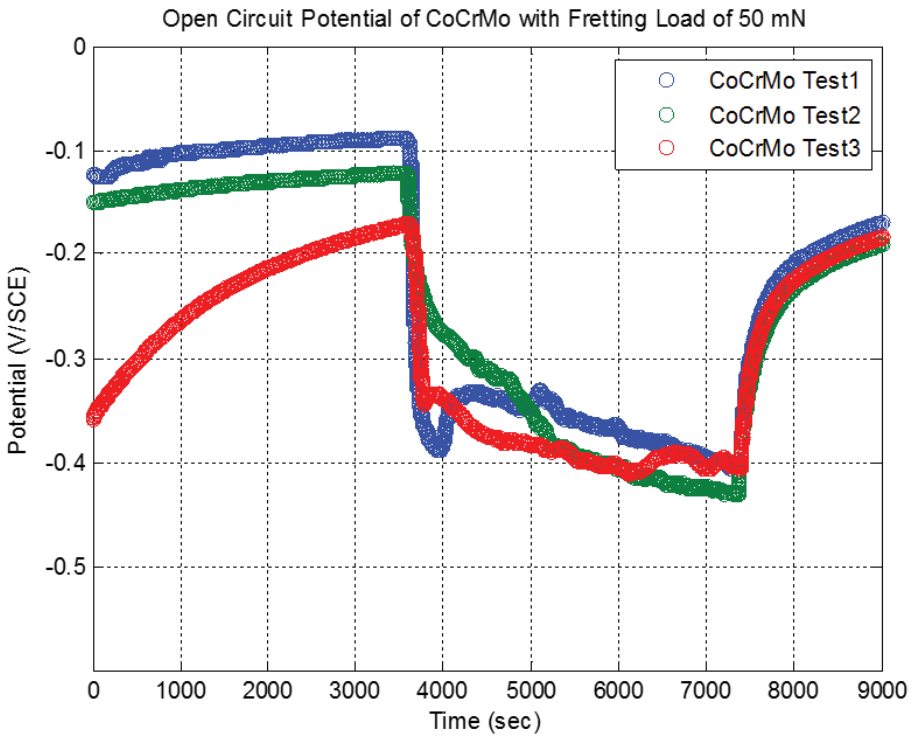

Figure 10: OCP Measured on CoCrMo at 50 mN

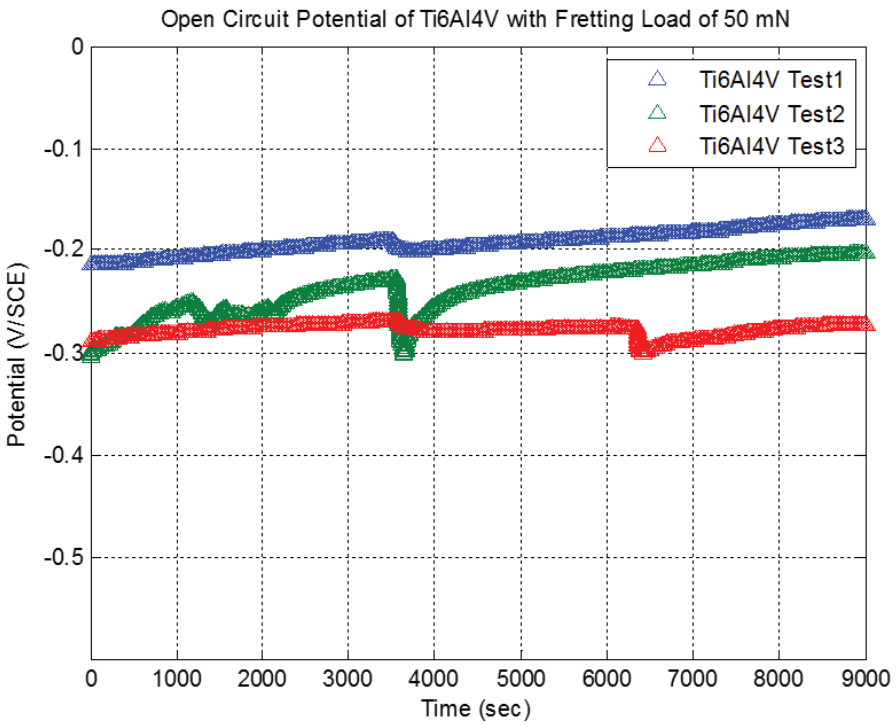

Figure 11: OCP Measured on Ti6Al4V 50 mN

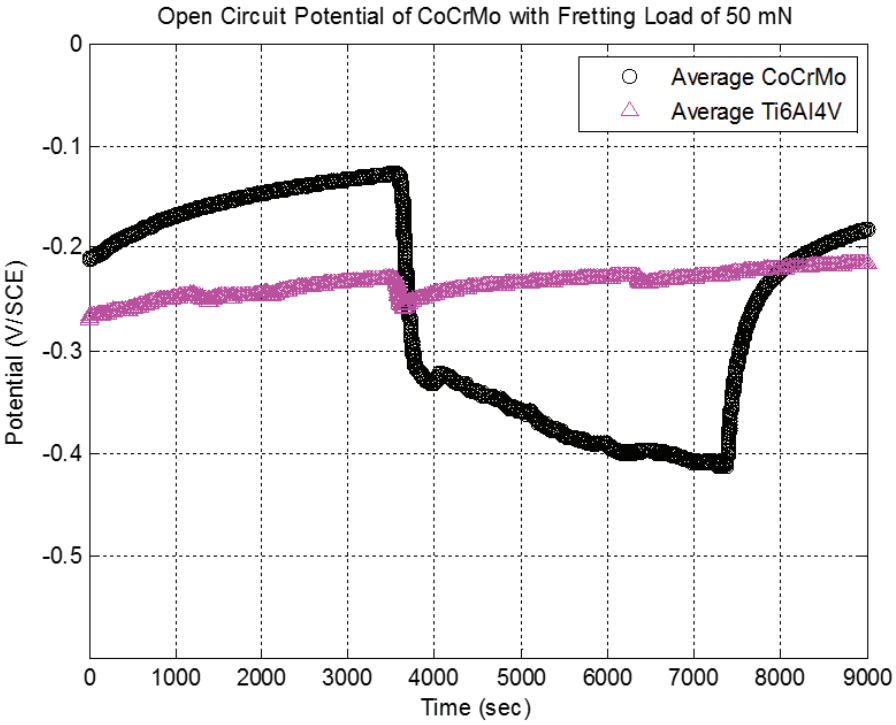

Figure 12: Average OCP on Ti6Al4V ELI and CoCrMo at 50 mN load

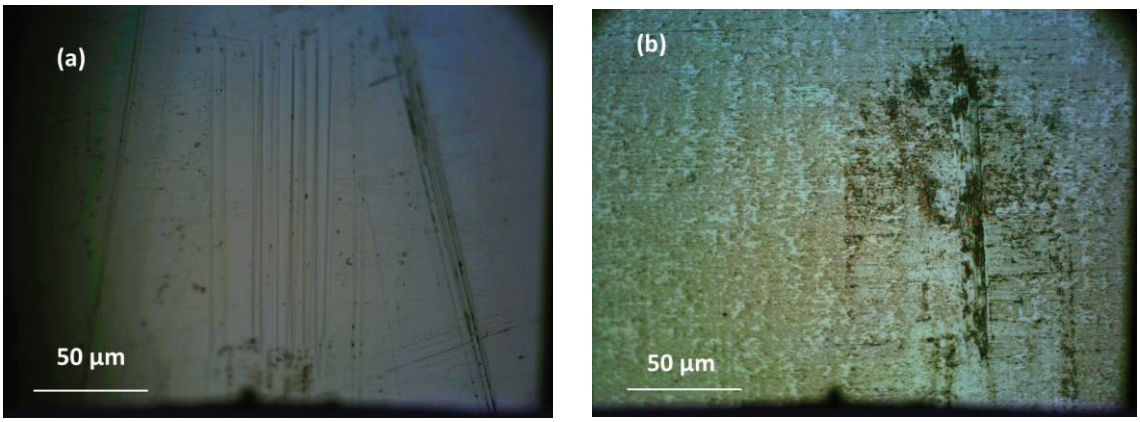

Figure 13: Optical microscope image at 50 mN (a) CoCrMo and (b) Ti6Al4V ELI

Figure 13 shows the optical microscopy image of the scratch at 50 mN. At the area of contact, the ball creates grooves that are parallel to the sliding direction. Pits of different sizes are visible in between these grooves. At Ti6Al4V ELI dark grey colored regions are found. These represent the corrosion debris composed mostly of oxide particles that are continuously formed on surface while scratching and removed from its place. These oxide flakes get crushed between surfaces during mechanical action and are embedded into fretting tracks. For CoCrMo less plastic deformation occurs and fretting marks are clearly visible. The pits on both surfaces are smaller and scratch are not much deep as compared to other loads. For Ti6Al4V the wear track is barely visible because of oxide layer embedded on the surface and is small in size when compared to CoCrMo. The fretted area undergoes extensive damage due to shear deformation and plowing of the ball. The surrounding of the fretted is smooth on which debris particulate is smeared all around.

The potential changes are summarized in Figure 14-15. The negative change describes oxide layer damage and therefore the anodic reaction (dissolution) is accelerated. As discussed, greater potential drops on CoCrMo are observed upon onset of fretting

contact. The drastic potential drop upon the fretting is followed by mild change in potential during successive fretting while less potential drop at the onset of fretting leads to continuous potential changes on CoCrMo surface. For Ti6Al4V surface the positive change of the potential would show its responsive repassivation produces strong oxide layer that can withstand the frictional forces during fretting. Therefore, the tribocorrosion behaviors of Ti6Al4V at a small sliding contact load are clearly superior to CoCrMo surface.

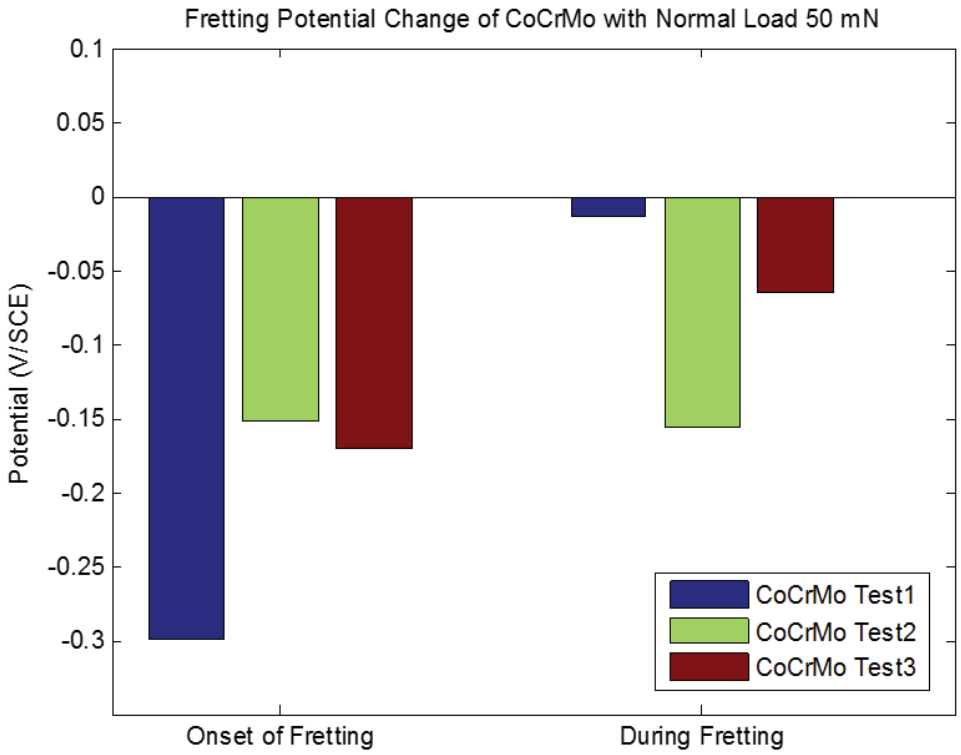

Figure 14: Statistical Analysis of OCP of CoCrMo at 50 mN

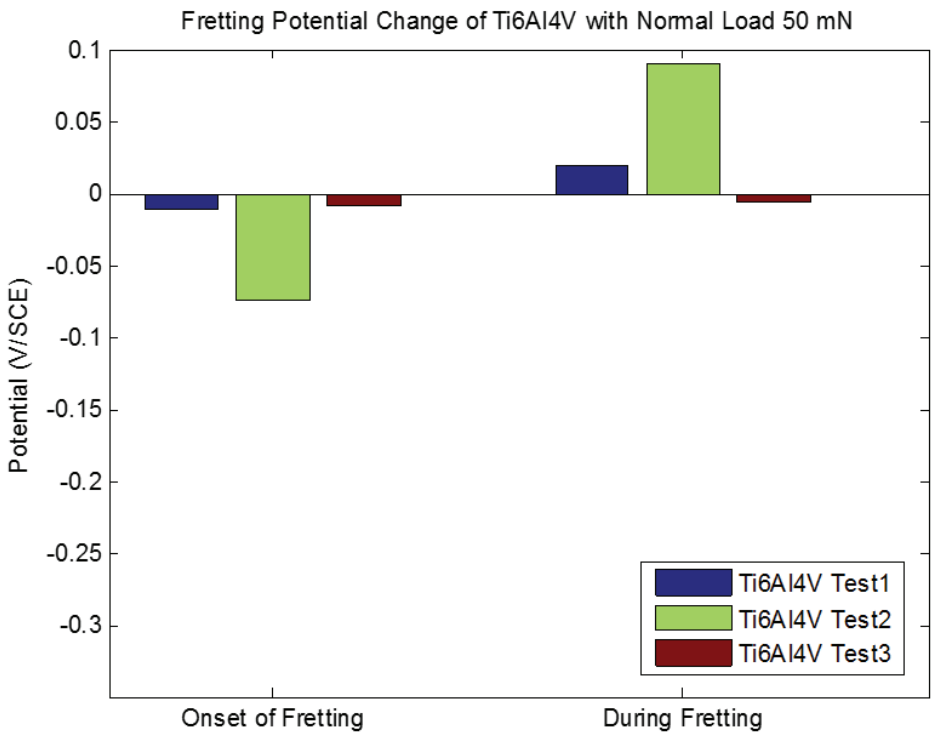

Figure 15: Statistical Analysis of OCP of Ti6Al4V at 50 mN

Evolution of coefficients of friction (COF) measured during fretting experiment in PBS is illustrated in Figures 16-22. It represents the ration between frictional force (tangential force) and normal loads during forwarding and backward motion of alumina sphere head. The slider motion was controlled at the same speed and length used in OCP measurements up to 1800 cycles. COF is closely related to the physical and chemical characteristic of the surface as well as the morphology of the surface including roughness and grain sizes at the small scale contact. Two different behaviors are observed during fretting with 50 mN normal loads on: in the early stage of sliding rapid increase from low COF values is followed by stable friction response with constant COF; while in case the high COF at the beginning of contact is obtained, COF gradually decreases with cycles. In

the initial stage of contact up to 20 mm of cumulative scratch distance, the COF values are around 0.45 and then increase up to 0.6 of COF and maintain steadily. If the COF values on COCrMo is as high as 0.6, then COF values gradually decrease until it reaches 0.5 on both forward and backward motions. The COF value is stable at an almost constant value throughout the rest of the test. In both cases, friction behavior tends to settle to a stable friction process on CoCrMo with 50 mN normal loads.

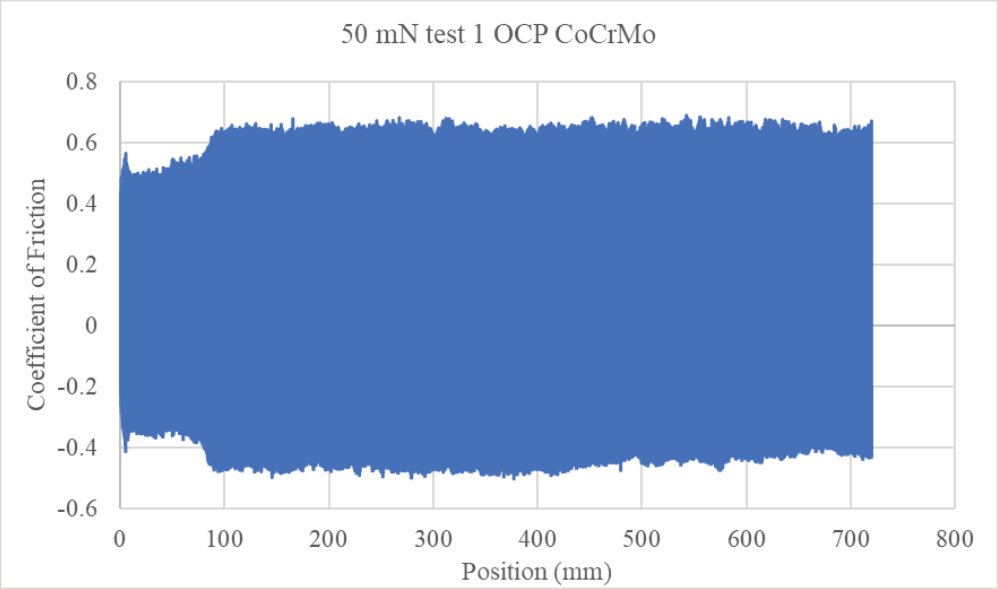

Figure 16: COF plot at 50 mN test 1 for OCP measurement on CoCrMo

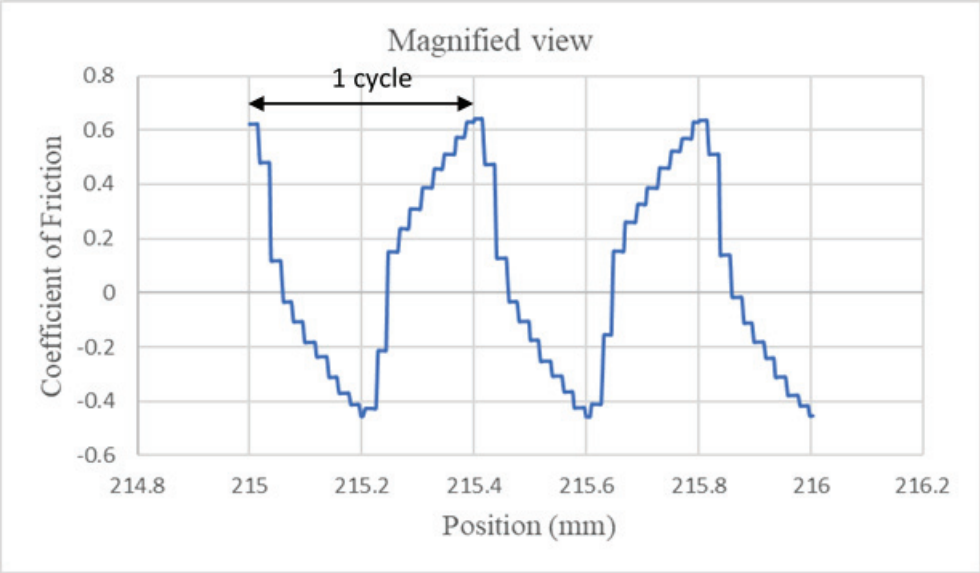

Figure 17: Magnified view of Figure 15 at random points

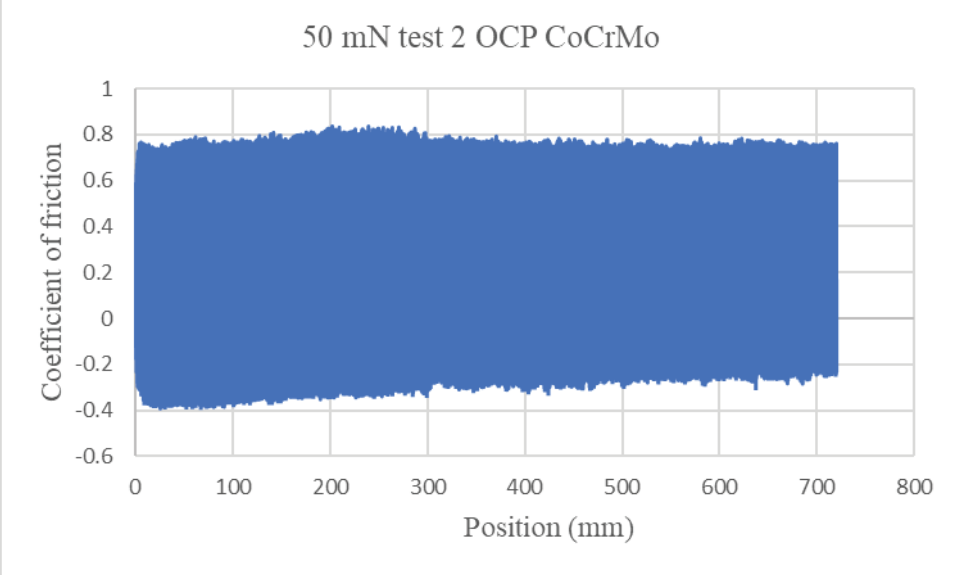

Figure 18: COF plot at 50 mN test 2 for OCP measurement on CoCrMo

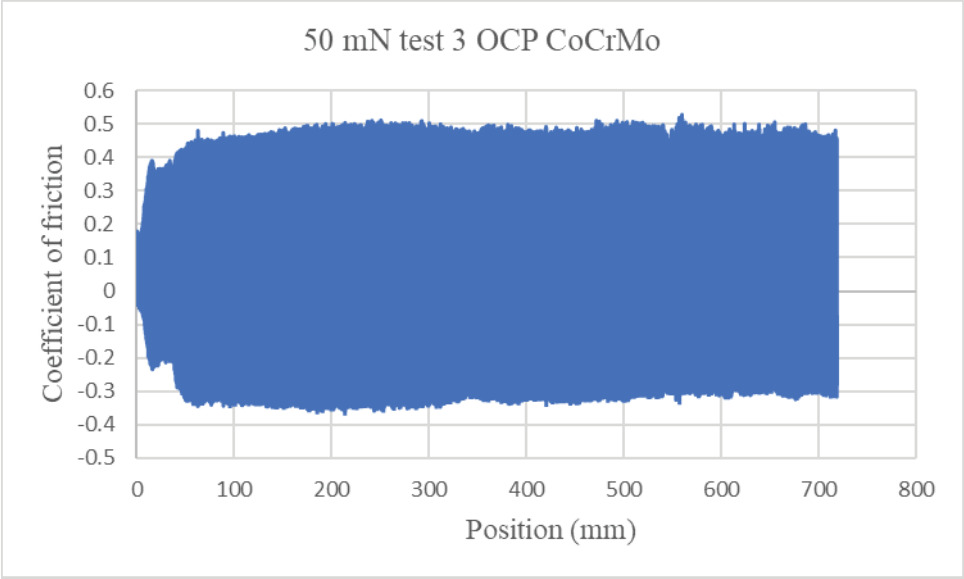

Figure 19: COF plot at 50 mN test 3 for OCP measurement on CoCrMo

COF changes on Ti6Al4V surface showed greater values of 0.6 from the beginning and maintain the value throughout the test. Similarly to the results from CoCrMo, the friction process at the high cycles presents steady responses. The minor increase in COF for both surface suggests locally damaged oxide layer may increase adhesive friction. From the micrographic analysis in Figure 13, wear debris effect on COF revolution is not significant.

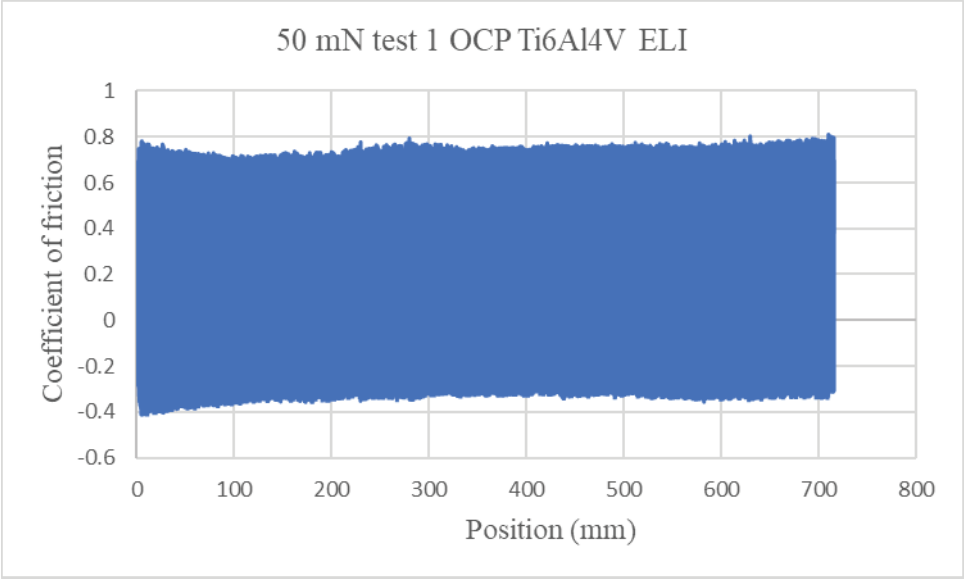

Figure 20: COF plot at 50 mN test 1 for OCP measurement on Ti6Al4V ELI

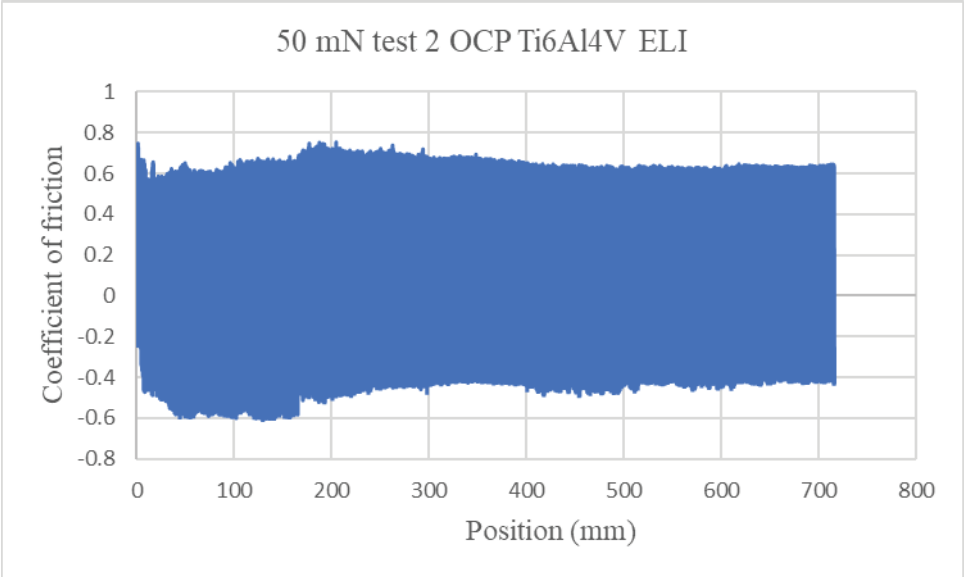

Figure 21: COF plot at 50 mN test 2 for OCP measurement on Ti6Al4V ELI

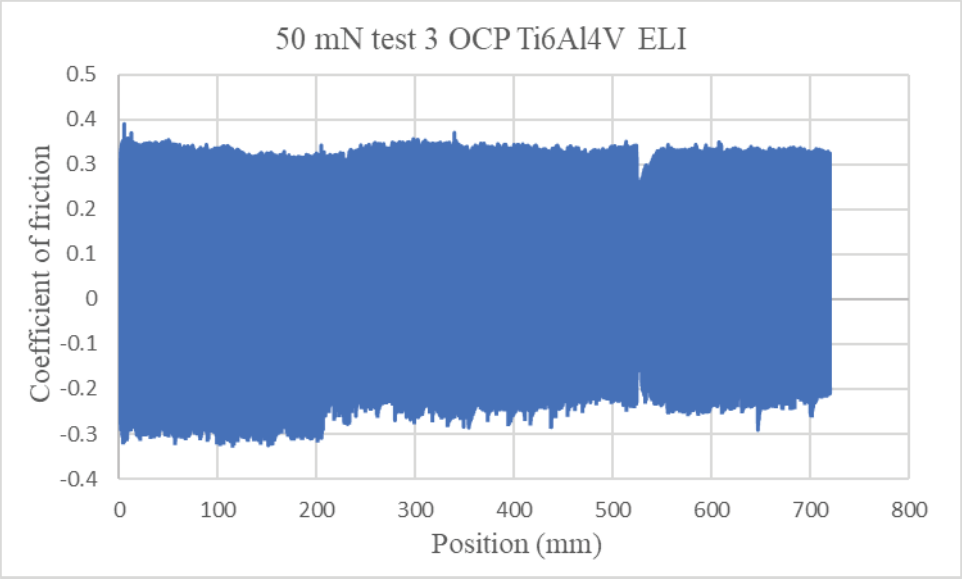

Figure 22: COF plot at 50 mN test 3 for OCP measurement on Ti6Al4V ELI

Table 8 summarizes the range of COF values at 50 mN on both surfaces. Average COF values for both metals at 50 mN are higher compared to COF values from greater normal loads at 100 mN and 200 mN.

Table 8: Maximum and Minimum COF values at 50 mN

Material	CoCrMo			Ti6Al4V ELI		
	Test 1	Test 2	Test 3	Test 1	Test 2	Test 3
Forward COF	0.69	0.84	0.52	0.81	0.75	0.39
Backward COF	-0.50	-0.39	-0.36	-0.41	-0.61	-0.33

3.1.2 For Normal Force 100 mN:

The change in potential was measured with a normal load of 100 mN (other parameters same as shown in experimental methodology) before the onset of fretting,

during fretting and after fretting motion stops for CoCrMo and Ti6Al4V ELI as shown in Figures 23-25. The potential was allowed to stabilize for 1 hour before fretting was initiated. Once the system is reached to a stable condition, the fretting is initiated with 100 mN load. OCP responses on CoCrMo at 100 mN normal load are similar to those of CoCrMo at 50 mN normal loads as discussed above. There is a rapid potential drop due to oxide layer damage upon the sliding motion. While the potential gradually decreased during fretting with 50 mN, however, potential values during fretting with 100 mN present stable phase with minor fluctuations from all the measurements.

As soon as the slider is addressed, there is a sharp drop in potential on Ti6Al4V ELI as shown in CoCrMo fretting corrosion experiments. However, the potential is rapidly increased with subsequent fretting contacts. It clearly illustrates the titanium oxide is capable of spontaneous recovery of the oxide film. The integrity of the reformed oxide layer is gradually improved during active slider motions, while the potential of CoCrMo during fretting settled at significantly low values. The initial OCP drop on Ti6Al4V at 100 mN was similar to that of CoCrMo at the same fretting loads, but as shown in Figure 25, Ti6Al4V surface presents it superior nature of oxide chemistry during fretting corrosion. The rate of passive layer recovery on CoCrMo is very rapid when the fretting motion is ceased. However, the rate of passivation on Ti6Al4V is almost continuous from the active fretting phase.

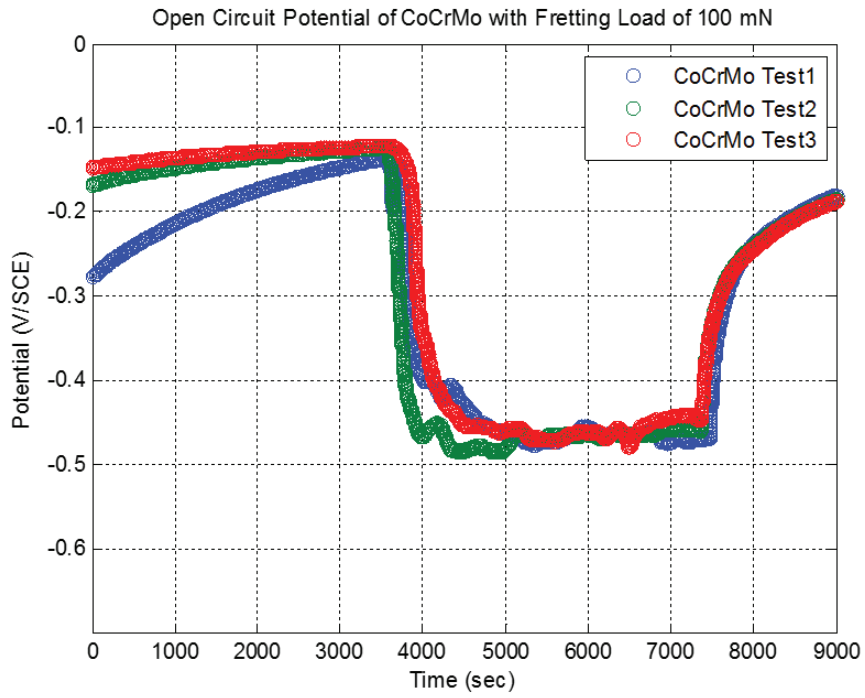

Figure 23: OCP measurement on CoCrMo at 100 mN load

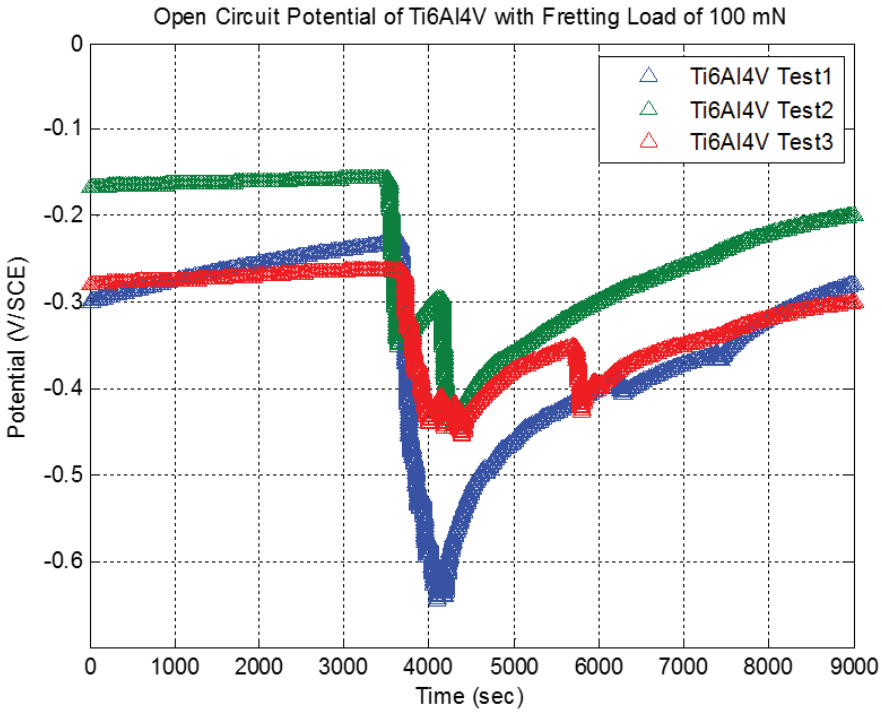

Figure 24: OCP measurement on Ti6Al4V ELI at 100 mN load

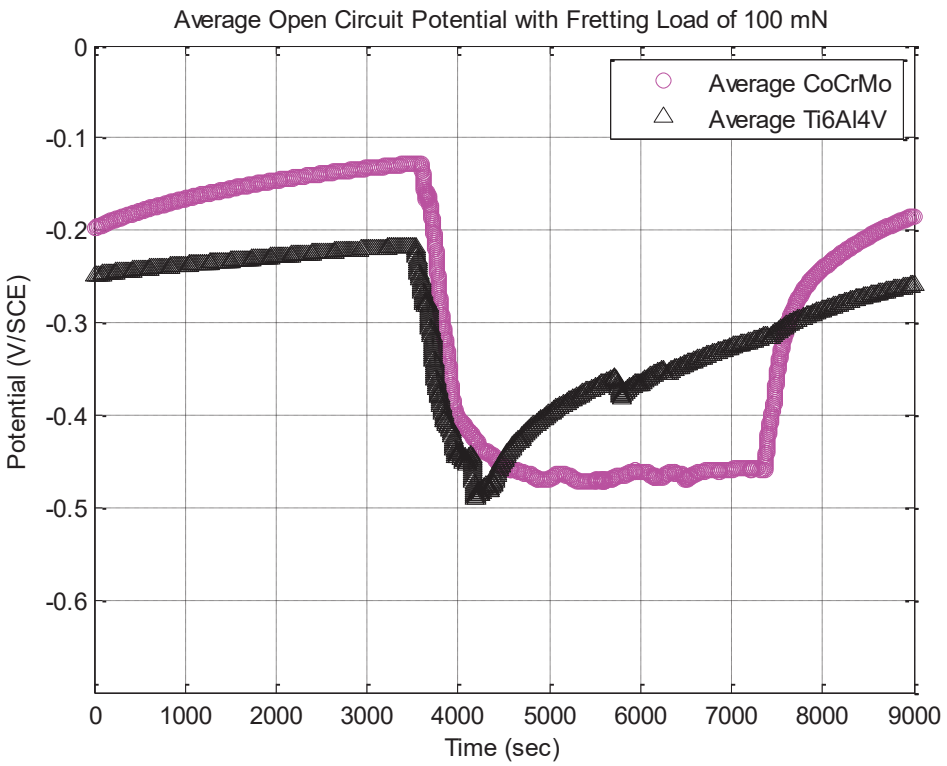

Figure 25: Average OCP measurement on CoCrMo and Ti6Al4V at 100 mN normal load

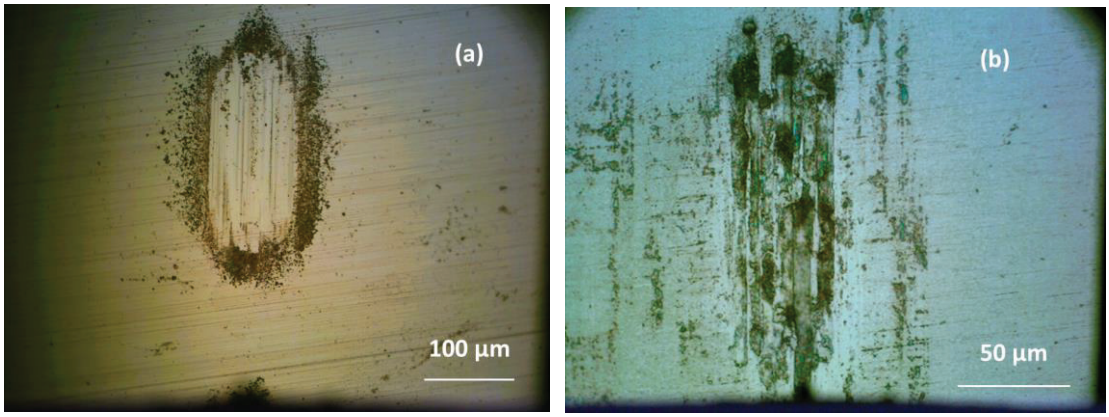

Figure 26: Optical microscope image at 100 mN (a) CoCrMo and (b) Ti6Al4V ELI

The micromorphologies on the damaged area by fretting with 100 mN normal loads are different from those from fretting contact at 50 mN as shown in figure 26. Especially,

Ti6Al4V surface illustrated wear tracks by metal surface abrasion and large scale plastic strains. Wear damages on CoCrMo presents pile-up of nano debris mainly produced from progressive plowing of the oxide layer. Dark areas with undulations of grooves at Ti6Al4V are found, while the wear trench of CoCrMo is surrounded by small metal oxide wear particles. The wear of CoCrMo represents the corrosion debris composed mostly of oxide particles that are continuously formed on surface while scratching and removed from its place. The wear flakes produced by fatigue contact on Ti6Al4V surface would be crushed at the subsequent sliding contacts and agglomerated into fretting tracks. At some point, these oxide flakes might get removed from the contacting surface and ball plows more metal from Ti6Al4V ELI due to which there are few more potential drops during OCP measurements. For CoCrMo less plastic deformation occurs and fretting marks are clearly visible. OCP changes at the onset of fretting and progress of fretting are summarized in Figure 27-28. OCP drops on both CoCrMo and Ti6Al4V are significant when the fretting contact is initiated. However, the capability of oxide layer reformation on Ti6Al4V is much superior to that of CoCrMo during active sliding contact. The positive change in Ti6Al4V illustrated the degree of active repassivation.

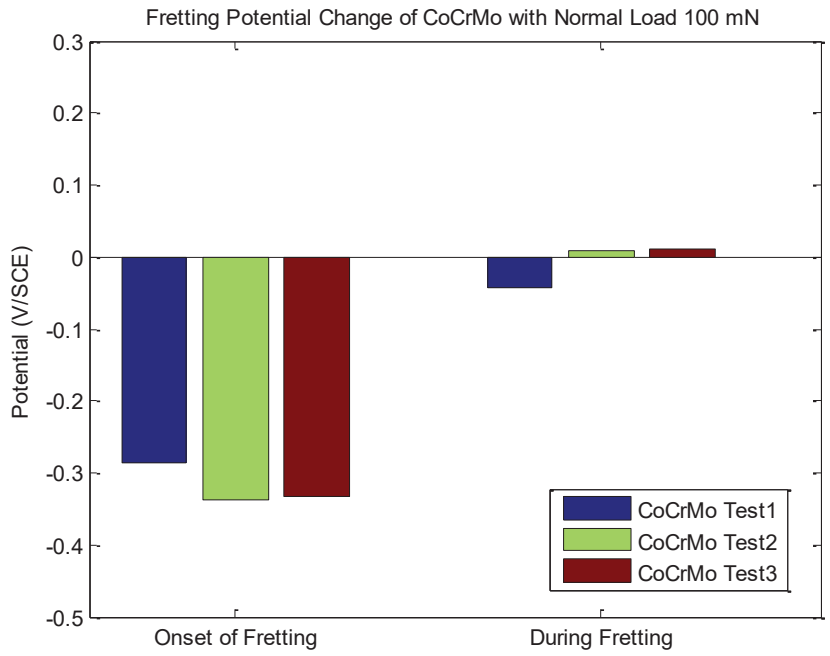

Figure 27: Statistical Analysis of OCP of CoCrMo at 100 mN

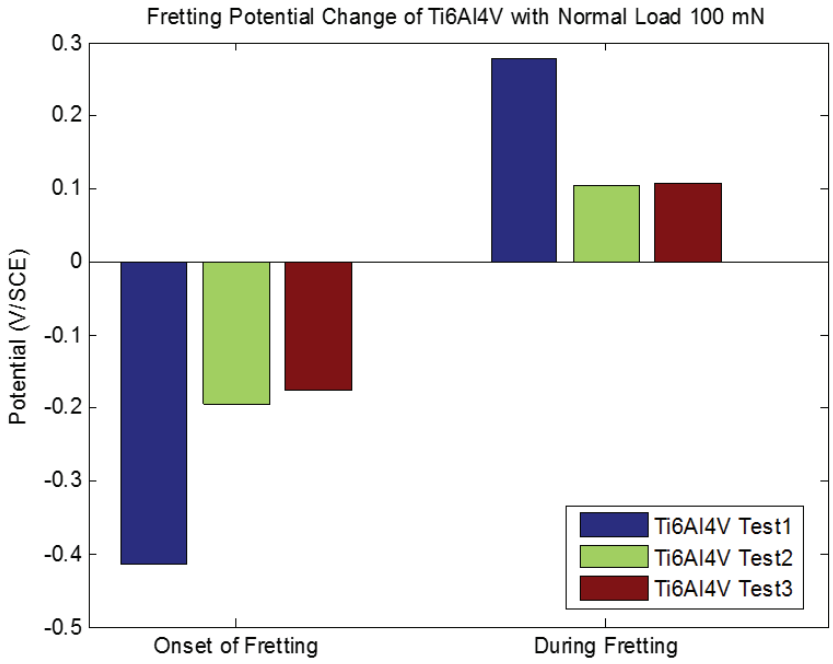

Figure 28: Statistical Analysis of OCP of Ti6Al4V at 100 mN

During its cumulated sliding distance, COF values rapidly increase up to 0.6 in the early 250 cycles and then progressively increases during the entire fretting process as can be seen in figure 29-34. When the fretting is ceased, COF values reach approximately 0.5. However, COF from Ti6Al4V surface illustrated more fractal behavior. The average COF values on Ti6Al4V is smaller than those on CoCrMo, but the results present unstable friction response. As discussed in micromorphologies on the damaged area, the result suggests a cycle of COF magnitude changes (alternating increase and decrease of COF) is due to a repeated pattern of large abrasive wear debris formation and rejection. The wear debris will be subjected to a large scale plastic deformation and oxidation that result in agglomerated hard and brittle wear particles. During the following mechanical loadings, the brittle debris may induce third-body friction. Therefore the result describes during the early fretting cycles mechanical loading significantly governs electrochemical response, while later fretting cycles the recovered oxide layer stabilizes the tribological response of the Ti6Al4V surface.

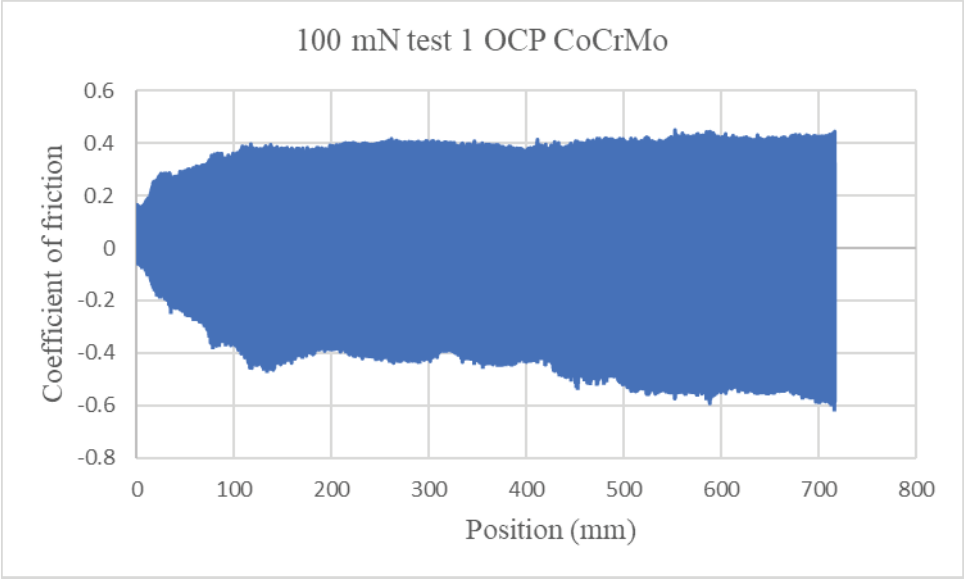

Figure 29: COF plot at 100 mN test 1 for OCP measurement on CoCrMo

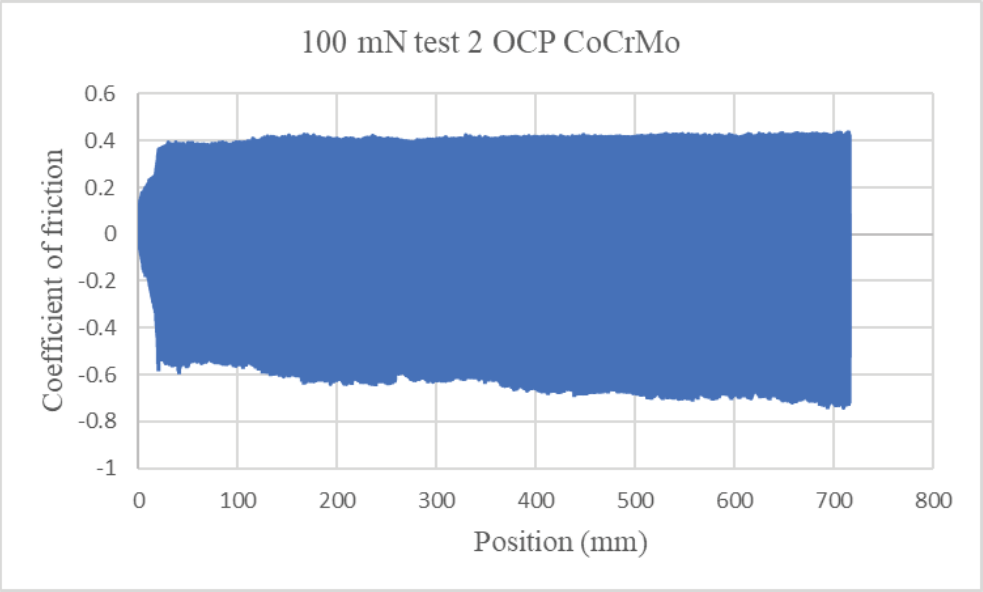

Figure 30: COF plot at 100 mN test 2 for OCP measurement on CoCrMo

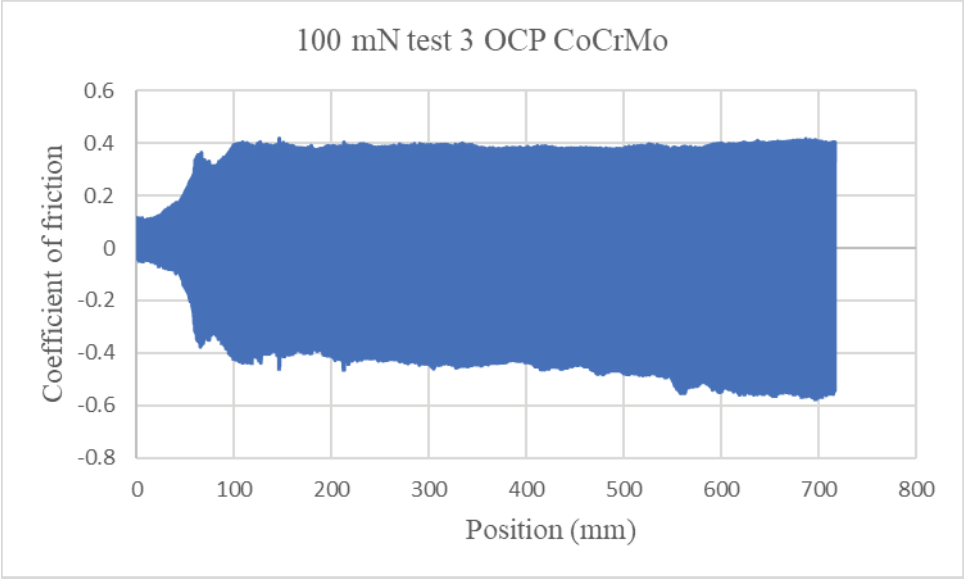

Figure 31: COF plot at 100 mN test 3 for OCP measurement on CoCrMo

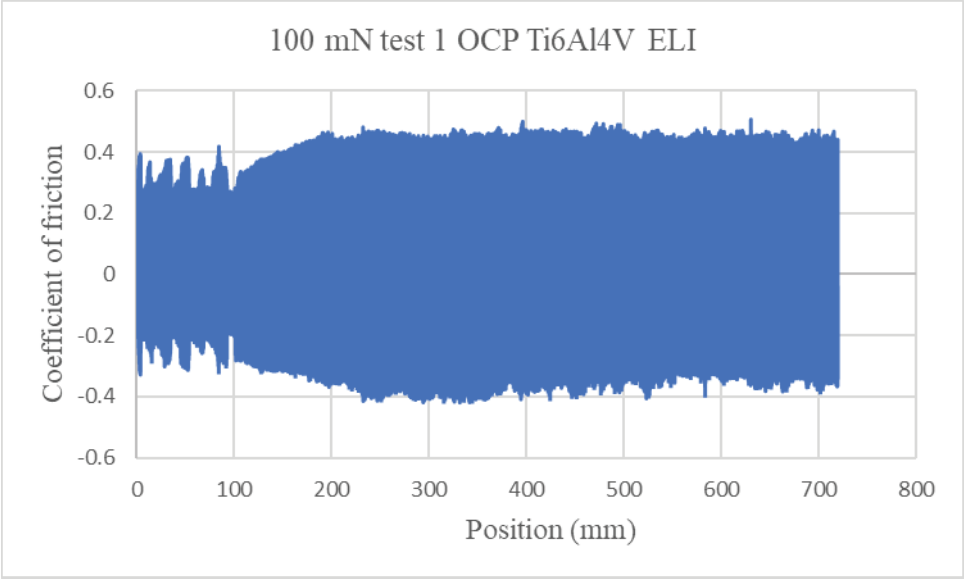

Figure 32: COF plot at 100 mN test 1 for OCP measurement on Ti6Al4V ELI

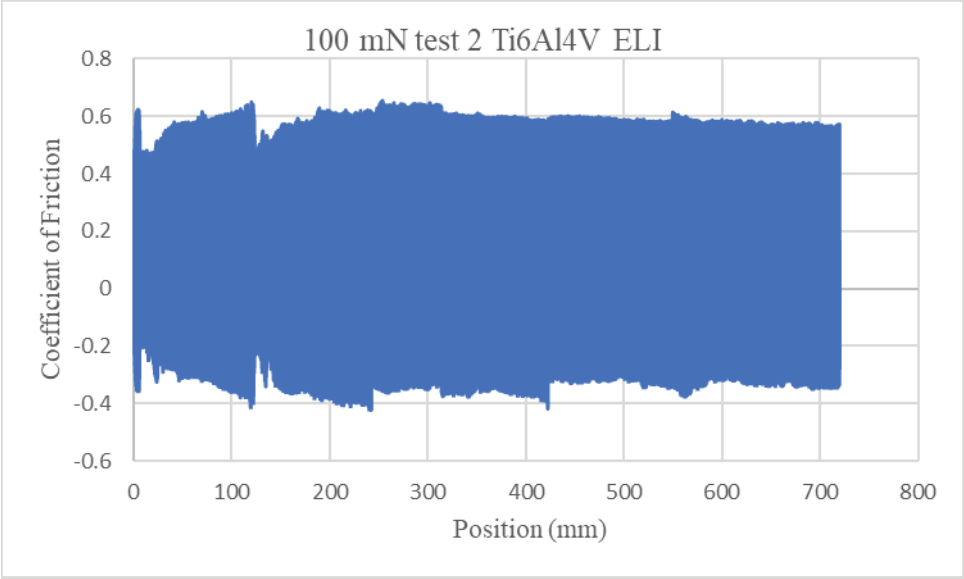

Figure 33: COF plot at 100 mN test 2 for OCP measurement on Ti6Al4V ELI

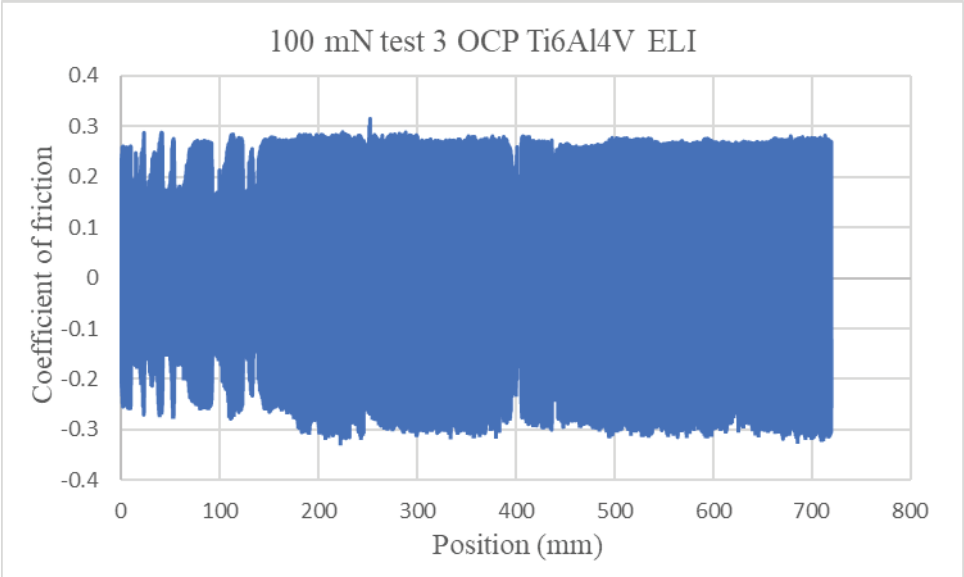

Figure 34: COF plot at 100 mN test 3 for OCP measurement on Ti6Al4V ELI

Table 9 shows the maximum and minimum values of COF at 50 mN. COF values for both metals were high at 50 mN when compared with other loads.

Table 9: Maximum and Minimum COF values at 100 mN

Material	CoCrMo			Ti6Al4V ELI		
	Test 1	Test 2	Test 3	Test 1	Test 2	Test 3
Forward COF	0.45	0.43	0.42	0.50	0.65	0.31
Backward COF	-0.61	-0.74	-0.57	-0.41	-0.42	-0.32

3.1.3 For Normal Force 200 mN:

The change in potential was measured with parameters the same as shown in experimental methodology. Three stages of measurements including before the onset of fretting, during active fretting, and after fretting motion stops were conducted on CoCrMo and Ti6Al4V surface with the normal load of 200 mN. The potential changes are depicted in Figures 35-37. The OCP responses on both CoCrMo and Ti6L4V at 200 mN are very similar to those at 200 mN in general. A large potential drop was obtained as soon as fretting contact is initiated. With different initial OCP before fretting starts, all the measured potential levels upon the fretting are mostly the same level at -0.56 V. During the active fretting motions, potentials on CoCrMo are stable with minor fluctuations until the fretting motion is ceased. Similarly, potential drops on Ti6Al4V was initiated upon the fretting motion. However, during the continuous fretting, the potential is increased rapidly and gradually with time. There were several significant changes of OCP on Ti6Al4V. It may be because of fatigue delamination of the surface layer due to continuous fretting contact. Subsurface cracks would progressively grow during cyclic frictional forces and reach a critical length. The plastically deformed surface layer would be flaked from subsequent sliding and the layer is separated from the surface. The drastic potential drops during fretting take place when the delaminated wear particle is produced. However, the

desirable nature of oxidative recovery on Ti6Al4V surface gradually increase the potential as the secure oxide film is formed.

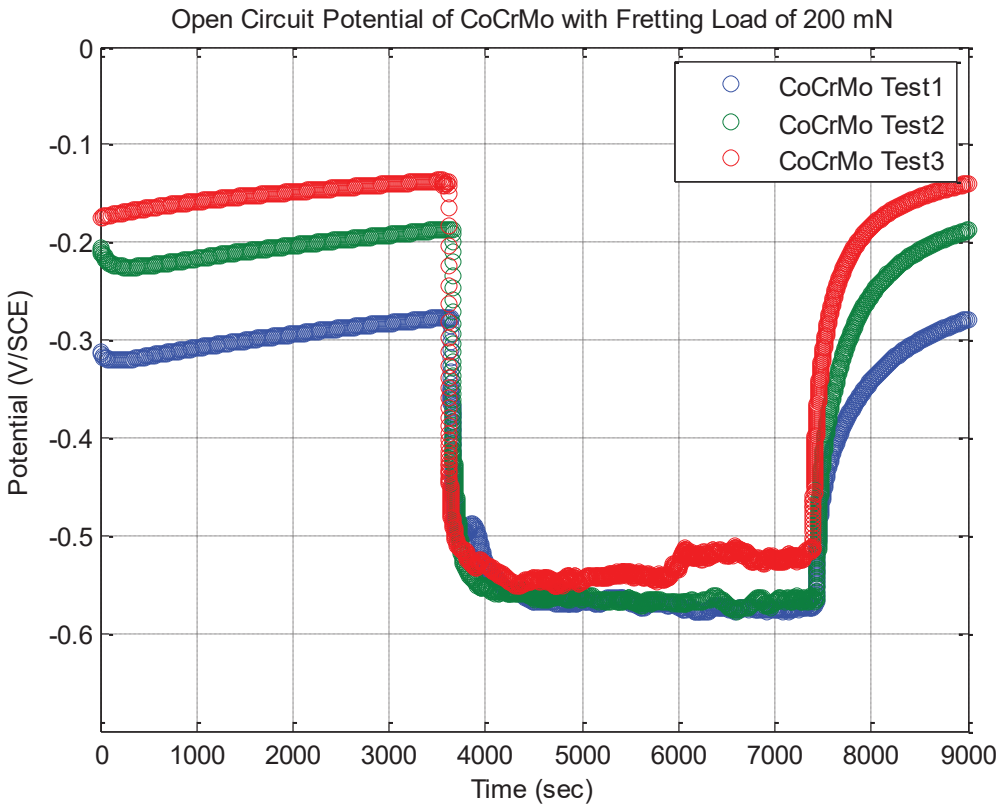

Figure 35: OCP Measurement on CoCrMo at normal load 200 mN

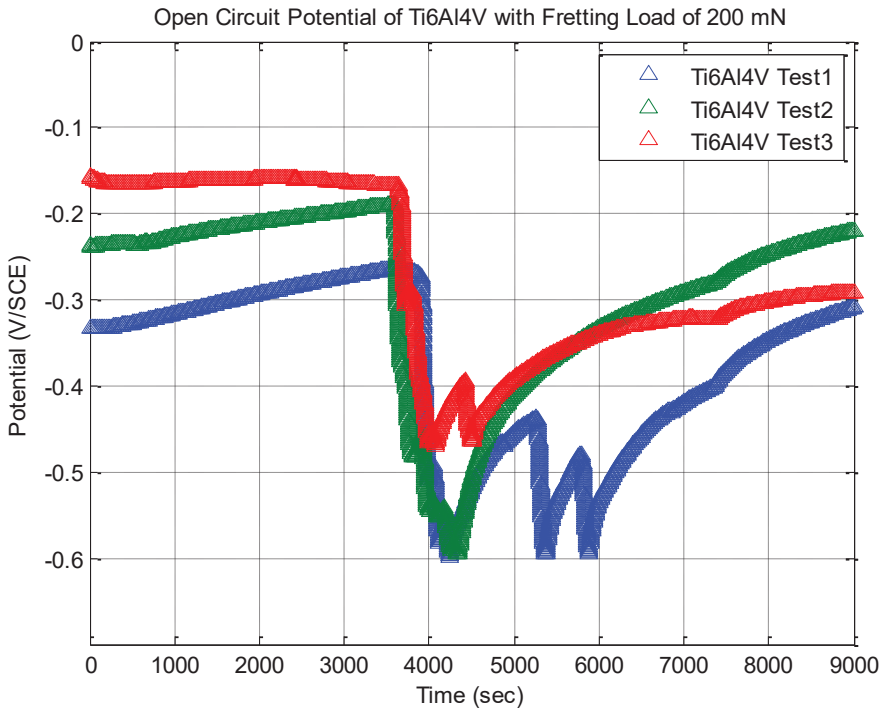

Figure 36: OCP measurement on Ti6Al4V ELI at 200 mN normal load

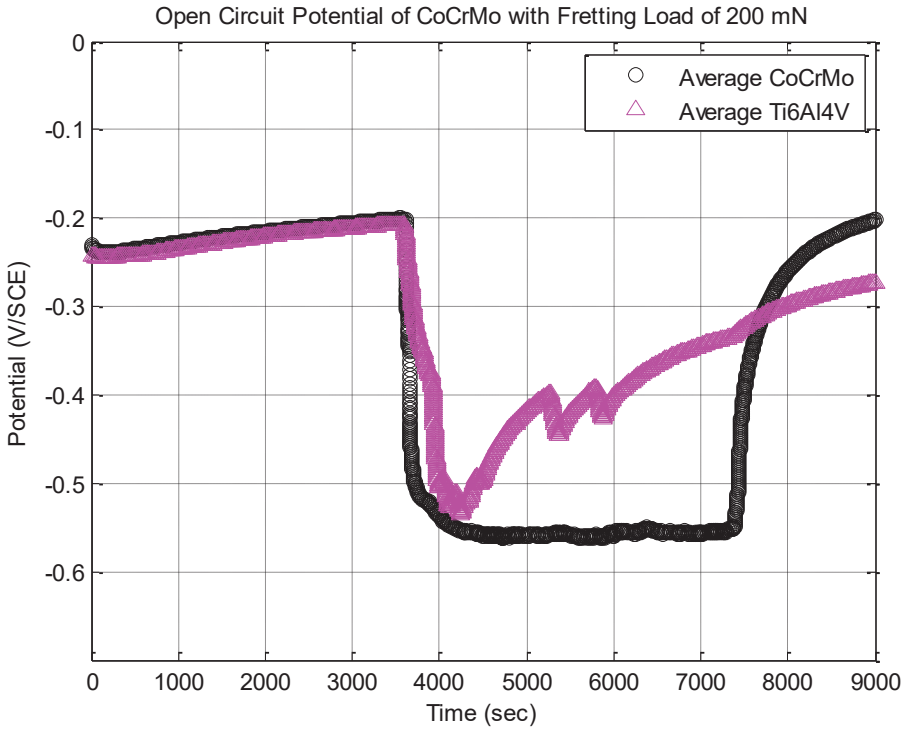

Figure 37: Average OCP measurement on Ti6Al4V ELI and CoCrMo at 200 mN load

Microscopic inspection of the damaged area as shown in Figure 38 illustrated a large material loss on Ti6Al4V surface. The morphology of damaged area on CoCrMo with 200 mN normal force is similar to that with at 100 mN normal loads. The nano-sized wear particle illustrated progressive oxidative wear process on chromium oxide, while the dark area of Ti6Al4V may present a large scale of plastic deformation and abrasive wear of subsurface layer. The unstable COF and OCP responses may be described as a contact fatigue damage as illustrated in delamination wear theory by Suh.

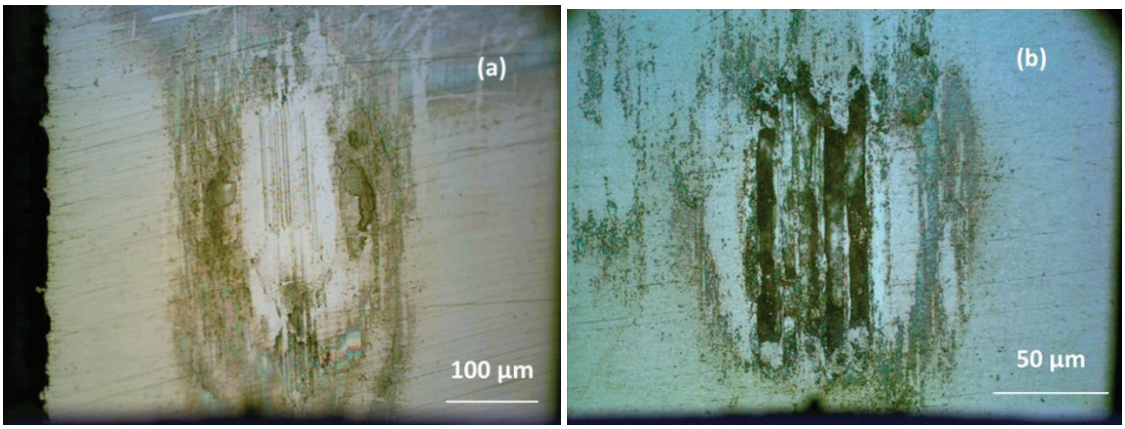

Figure 38: Optical microscope image at 200 mN (a) CoCrMo and (b) Ti6Al4V ELI

Figure 39-40 shows the OCP changes by fretting. As presented in the previous section with 100 mN, a dramatic drop os potential was observed when the fretting contact is initiated on both CoCrMo and Ti6AL4V surface. However, the positive potential obtained on Ti6Al4V describes the spontaneous repassivation of titanium oxide even during active sliding contact. The oxidation chemistry on both surfaces triggered by fretting is insensitive with higher normal loads at 100 mN and 200 mN.

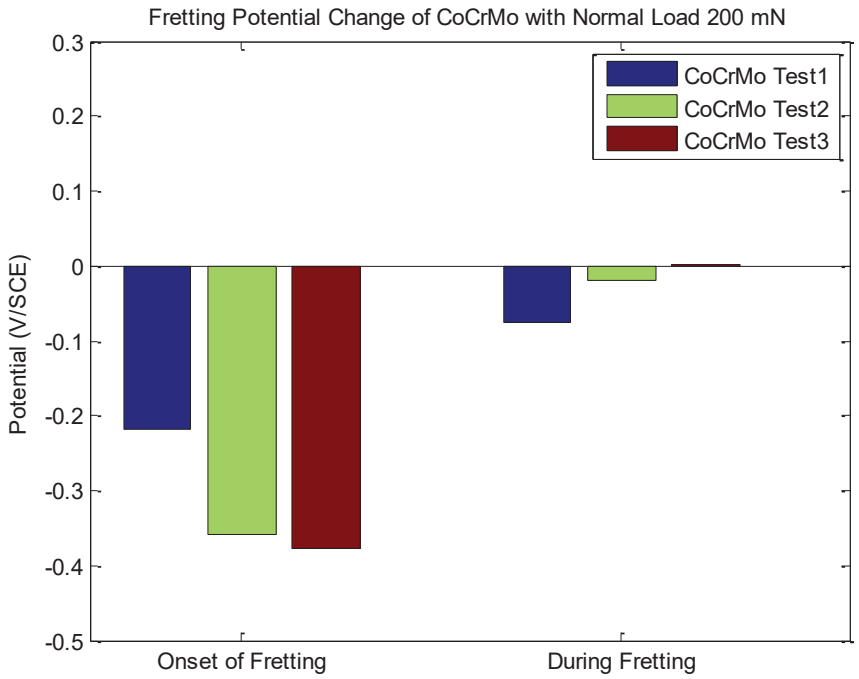

Figure 39: Statistical Analysis of OCP of CoCrMo at 50 mN

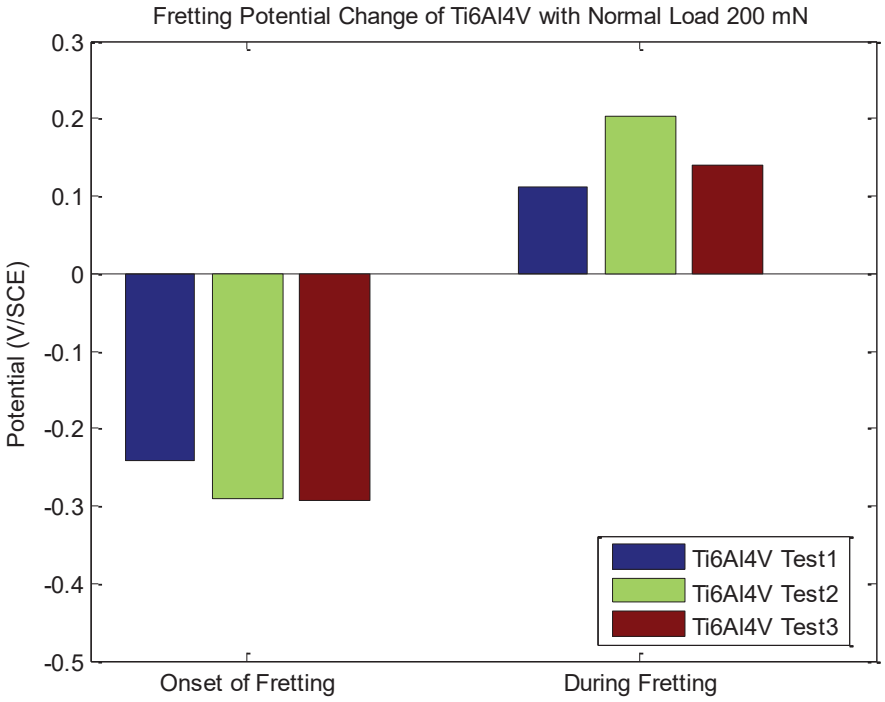

Figure 40: Statistical Analysis of OCP of Ti6Al4V at 50 mN

However, friction responses are significantly modified with an increased normal load as can be seen in figure 41-46. COF values on CoCrMo instantaneously reached a steady level of COF, approximately 0.4. Throughout the fretting process, COF values on CoCrMo is very stable and almost constant. This stable COF values may be well explained by the micromorphology of wear damage in Figure 38. The nano debris progressively produced by fretting without complete spalling of breakage of the oxide layer. However, the unstable COF changes on Ti6AL4V, as described before with 100 mN normal loads, is because of delamination wear by fretting. Evolution of OCP and COF during microcracking is invisible, but once the delamination wear particle is produced, a rapid increase of OCP and COF was observed. It is evident the fretting cycles at OCP drops is simultaneous with COF changes.

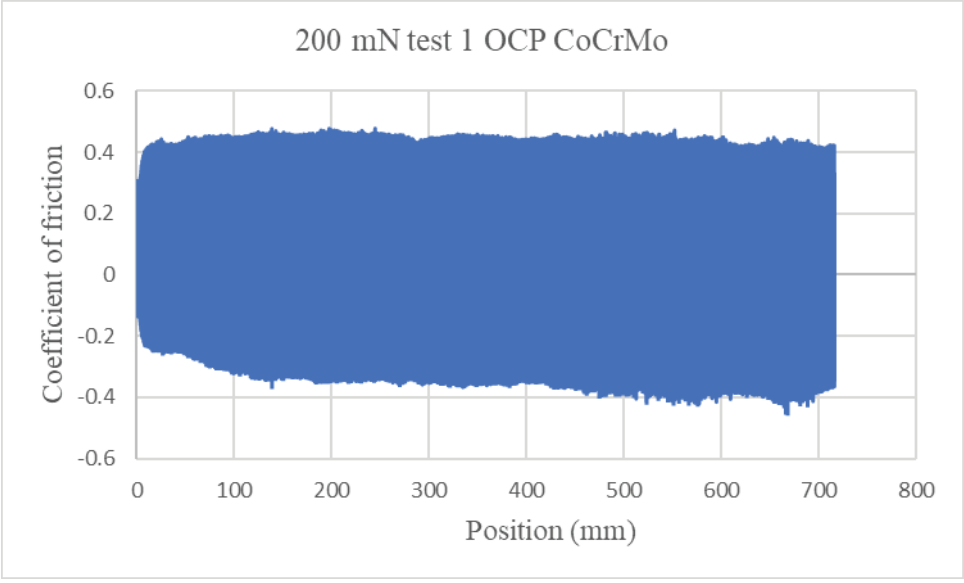

Figure 41: COF plot at 200 mN test 1 for OCP measurement on CoCrMo

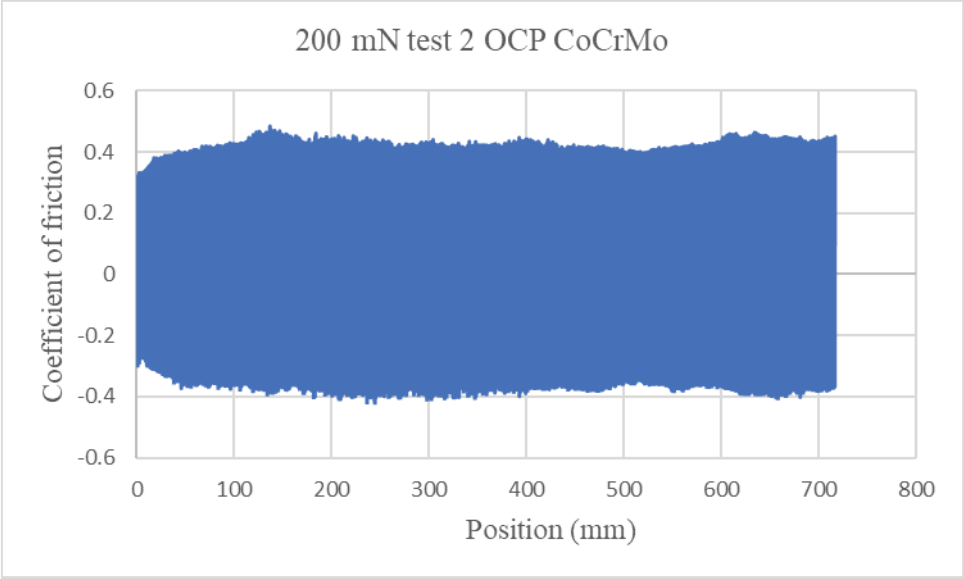

Figure 42: COF plot at 200 mN test 2 for OCP measurement on CoCrMo

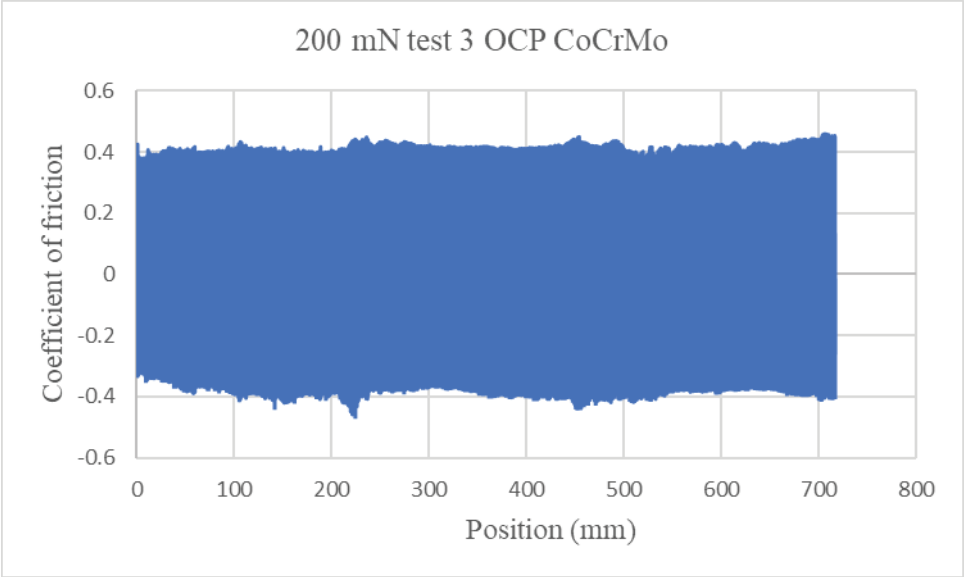

Figure 43: COF plot at 200 mN test 3 for OCP measurement on CoCrMo

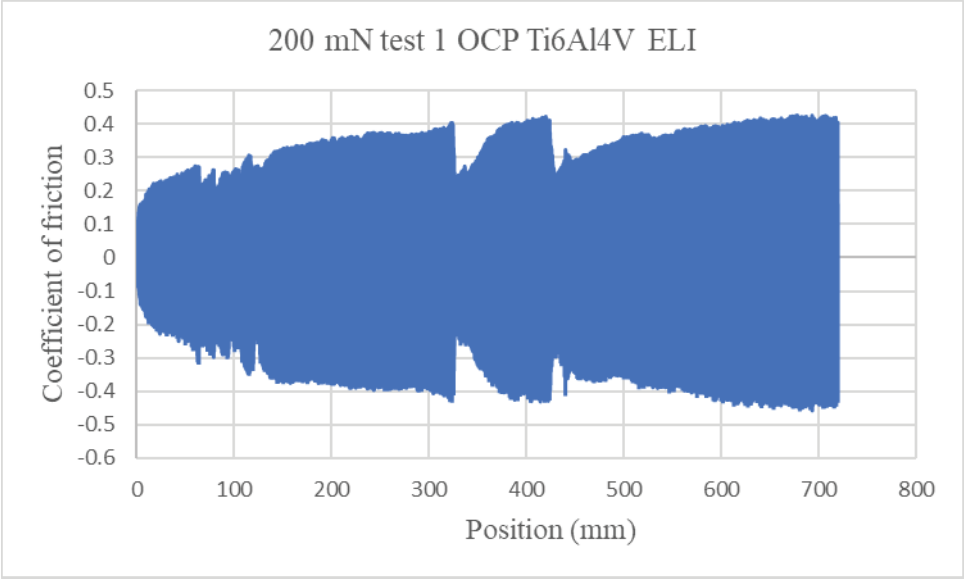

Figure 44: COF plot at 200 mN test 1 for OCP measurement on Ti6Al4V ELI

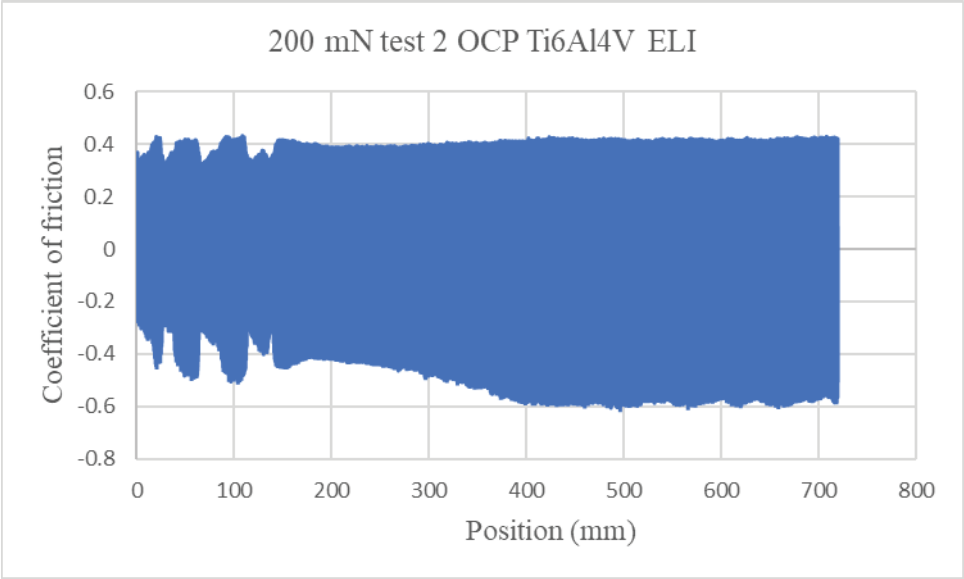

Figure 45: COF plot at 200 mN test 2 for OCP measurement on Ti6Al4V ELI

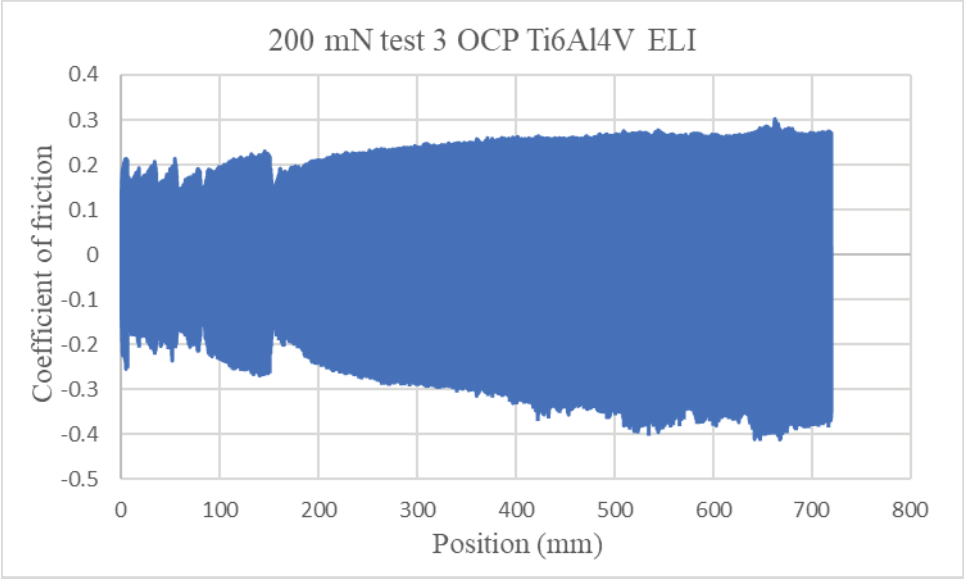

Figure 46: COF plot at 200 mN test 3 for OCP measurement on Ti6Al4V ELI

Table 10 shows the maximum and minimum values of COF at 50 mN. COF values for both metals were high at 50 mN when compared with other loads.

Table 10: Maximum and Minimum COF values at 200 mN

Material	CoCrMo			Ti6Al4V ELI		
	Test 1	Test 2	Test 3	Test 1	Test 2	Test 3
Forward COF	0.47	0.48	0.45	0.42	0.43	0.3
Backward COF	-0.45	-0.41	-0.46	-0.45	-0.61	-0.4

OCP changes during fretting at three different levels of normal loads on CoCrMo and Ti6AL4V are summarized in Figure 38-39. The different tribocorrosion behavior of Ti6Al4V and CoCrMo could be explained as the greater hardness and brittle oxide on CoCrMo prevents the surface from plastic deformation and abrasive wear, and therefore the adhesive contact with shearing motions of the slider would be dominant wear mechanism. A large plastic strain on Ti6Al4V would promote oxidation chemistry of titanium surface to facilitate the secure oxide film, and at the same time, slow

microcracking at the subsurface would delay the removal of the oxide layer. Finally, Ti6Al4V may present superior tribocorrosion property in general.

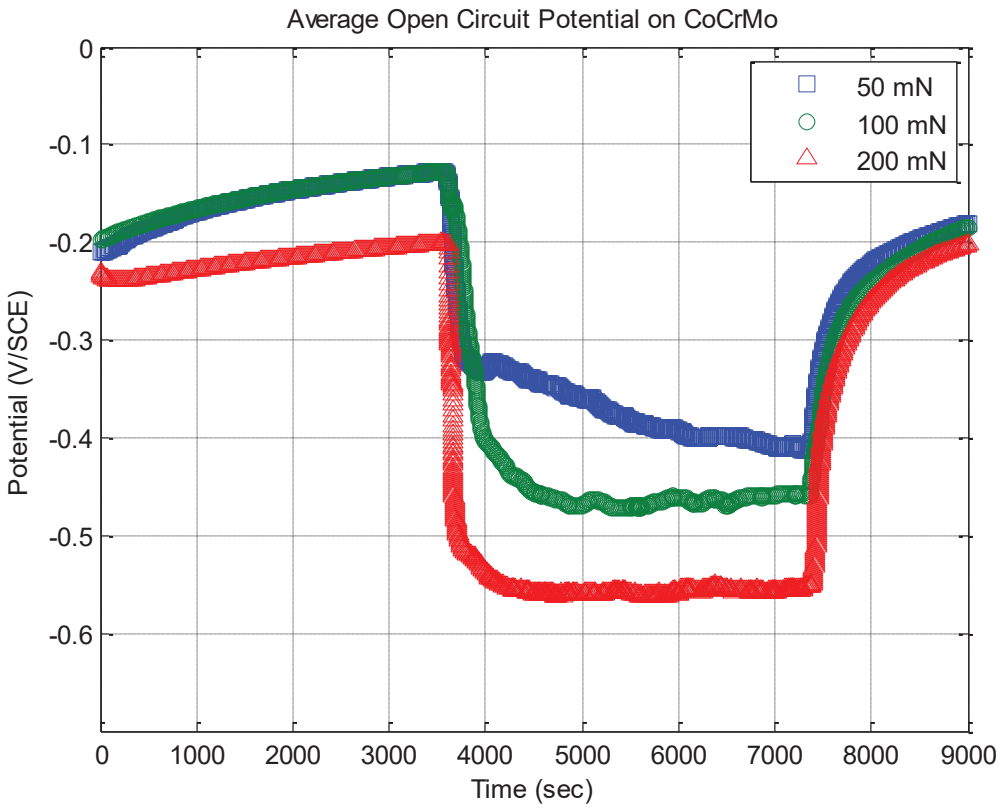

Figure 47: Average OCP plot on CoCrMo at various loads

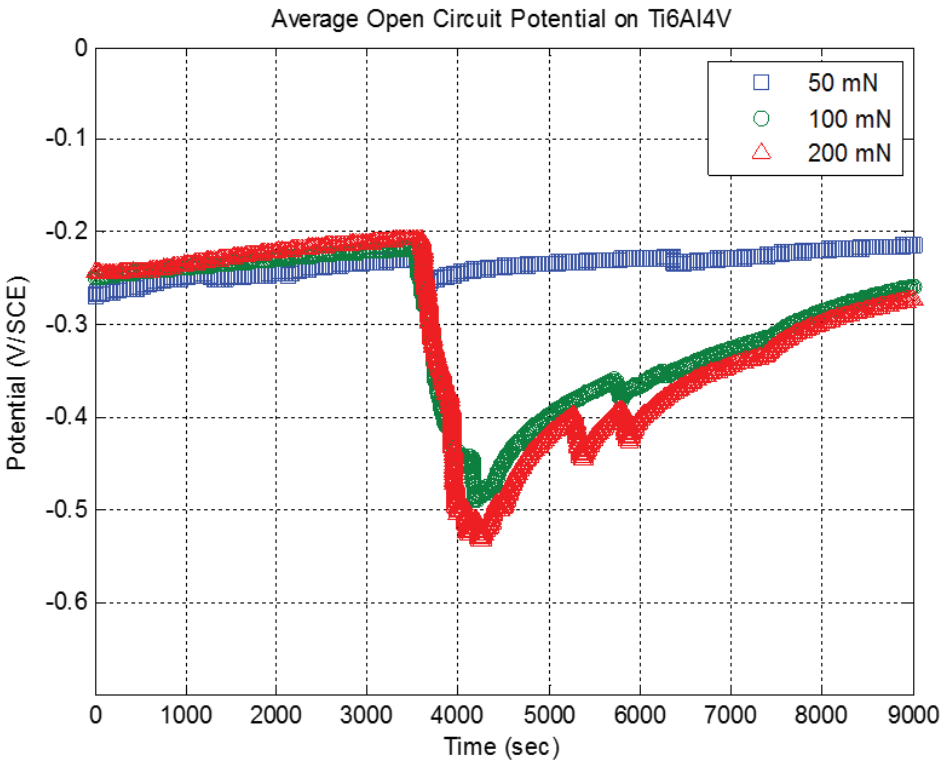

Figure 48: Average OCP plot on Ti6Al4V at various load

3.2 Potentiodynamic Polarization Resistance (PPR):

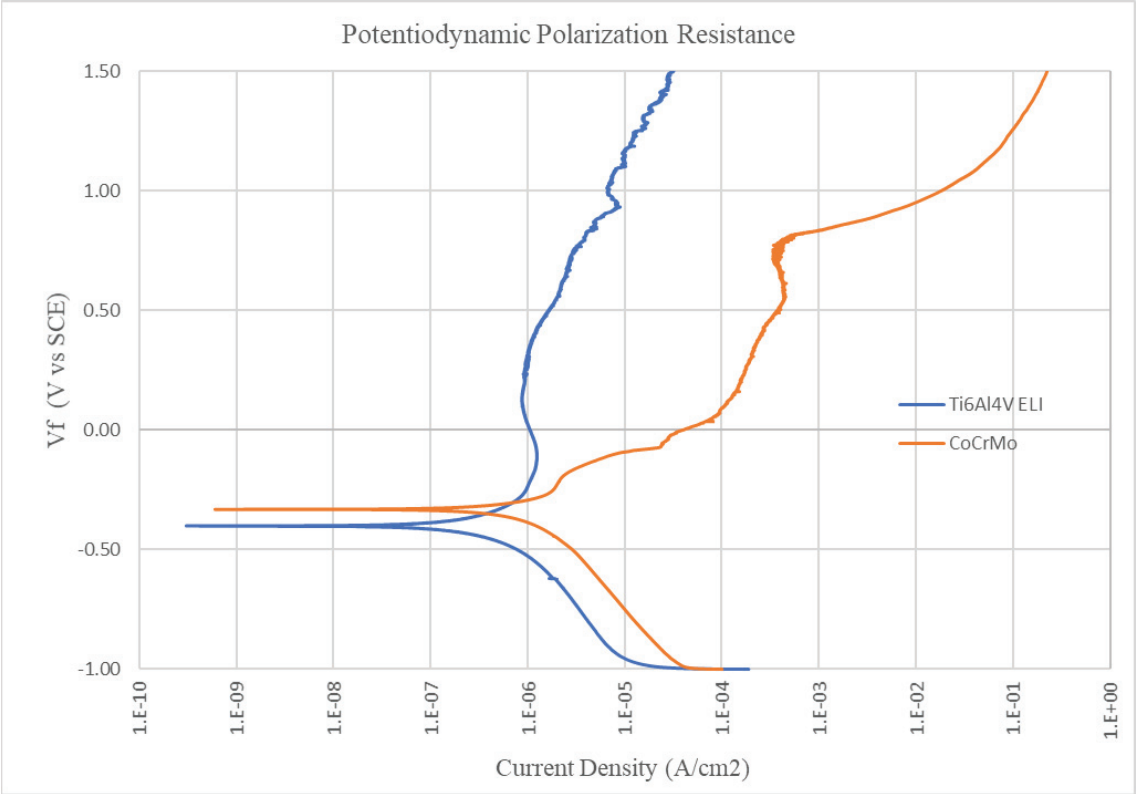

Figure 49: PPR plot

Figure 49 shows the potentiodynamic curves of both metals in PBS without scratching. Polarization curves are divided into four potential domains. In cathodic domain, the current density is due to the reduction of water and partially dissolved oxygen. The transition domain from cathodic to anodic current takes place at the corrosion potential (E_{corr}), at which the corrosion current density (i_{corr}) is obtained. Tafel slope is used to calculate E_{corr} and i_{corr} values. The third domain passive domain corresponds to the passive zone due to oxide formation on the metal surface and where the current density remains stable at the passive current density (i_p)[51]. Transpassive domain corresponds to the area

above the breakdown potential (E_b), characterized by the increase in current due to the dissolution of the protective oxide film as well as water oxidation[51].

CoCrMo showed the E_{corr} value of -0.331 V which was the same observed in OCP measurement before fretting was initiated. For Ti6Al4V ELI the E_{corr} value was -0.400 V. For potential values above + 0.75 V an increase in current density took place. This shows the dissolution of the oxide layer of CoCrMo. Whereas for Ti6Al4V ELI the passive domain was very large and spontaneous, and it did not show transpassive region at all where the dissolution of the passive film occurs rather it stayed in the active-passive zone. CoCrMo was more on the active side than passive and had transpassive zone where there was only increase in current after +0.75 V. The i_{corr} value of CoCrMo at 2.09e-6 A/cm^2 that was one order of magnitude higher than Ti6Al4V ELI which showed i_{corr} value of 3.1e-7 A/cm^2 which signifies that the corrosion rate of CoCrMo is higher when there is no load applied on it[40]. The formula for Corrosion rate (CR) is:

$$CR = \frac{3272\ x\ i_{corr}\ x\ Equivalent\ Weight}{Density}\ \frac{mm}{A\ cm\ year}$$

3.3 Potentiostatic Polarization test:

Potentiostatic Polarization tests were performed at three potential voltages at -0.5, 0.0, and +0.5 V with all three loads of 50 mN, 100 mN, and 200 mN on both alloys during fretting contact using the parameters as explained in the experimental procedure. Figure 50 represents current density change against potentials applied to CoCrMo during 50 mN fretting contact. During the test, the current reached stable values known as baseline current density (up to 600 seconds before fretting is initiated). The baseline current depends upon the surface condition during the time of test and the electrolyte. The current values change

from negative to positive when applied potentials from negative to positive. However, the current does not change due to fretting contact with the low normal load of 50 mN throughout the test period. Therefore, the small load may not induce significant oxidation chemistry on CoCrMo surface. This result is in accordance with the micromorphology of the damaged area as illustrated in Figure 13.

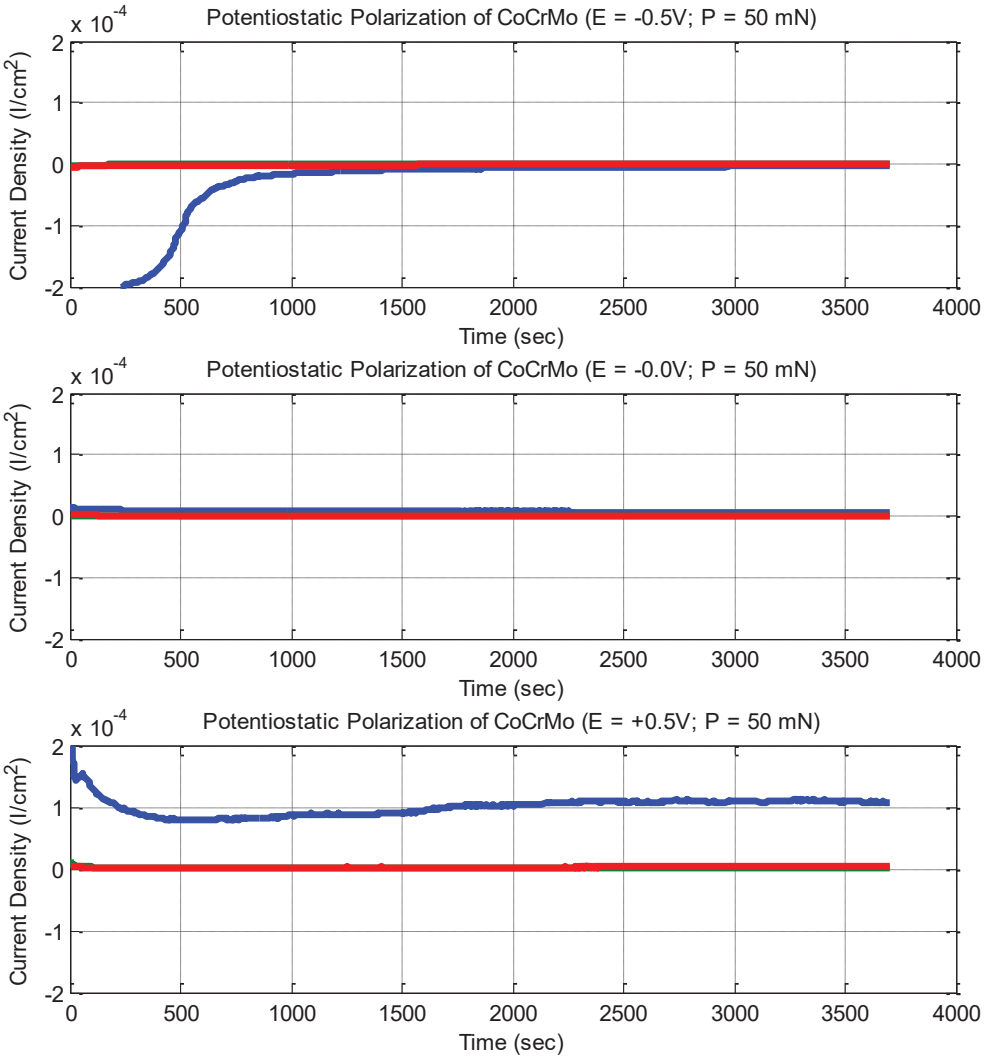

Figure 50: Potentiostatic Polarization of CoCrMo with 50 mN of fretting loading

Evolution of current density on CoCrMo with 100 mN fretting load is presented in Figure 51. The current density with negative potential presents no distinct change even with active fretting motions. This negative potential improved electrochemical stability of the chromium oxide layer. However, without potential and with the positive potential it is evident the current density increased instantaneously. This rise in current density indicates the magnitude of metal dissolutions by the exposure of metal beneath the oxide layer.

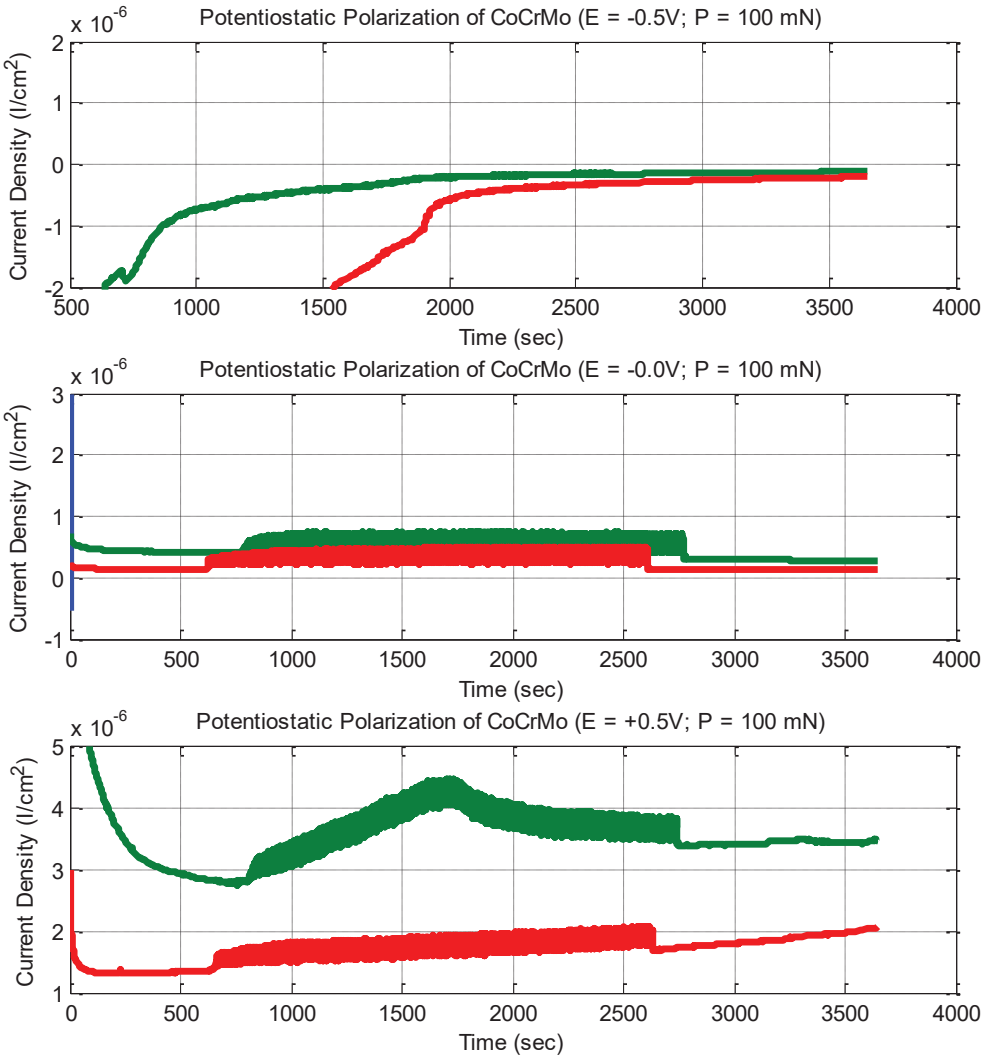

Figure 51: Potentiostatic Polarization of CoCrMo with 100 mN of fretting loading

Figure 52 represents current density on CoCrMo change during highest fretting load with 200 mN. Similarly to previous observation with 100 mN fretting load, baseline current moved from negative values to positive values with potentials from negative to positive. After the stabilized baseline current is obtained, the fretting load was applied while monitoring current changes. It is more evident the increase in current density at +0.5 V potential is greater than the current density without potential applied (0.0 V).

A series of current density measurement was performed on Ti6Al4V at the same potential values and fretting loading. All the results presented in Figures 53-55 indicate insignificant current change at all potentials and fretting loads. The results confirmed that the oxidation chemistry of titanium is not sensitive against electrochemical and mechanical stimuli. It may conclude Ti6Al4V implants would be superior in tribocorrosion damage process.

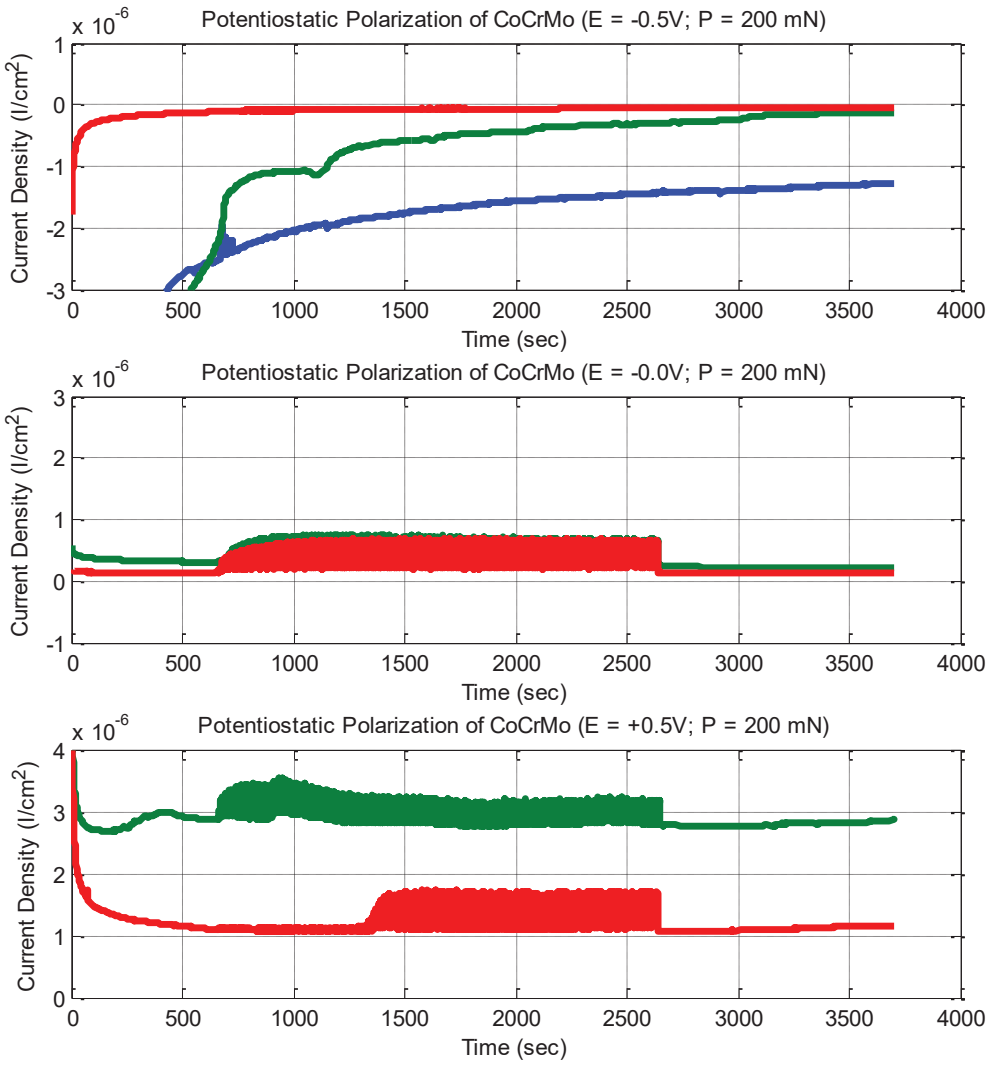

Figure 52: Potentiostatic Polarization of CoCrMo with 200 mN of fretting loading

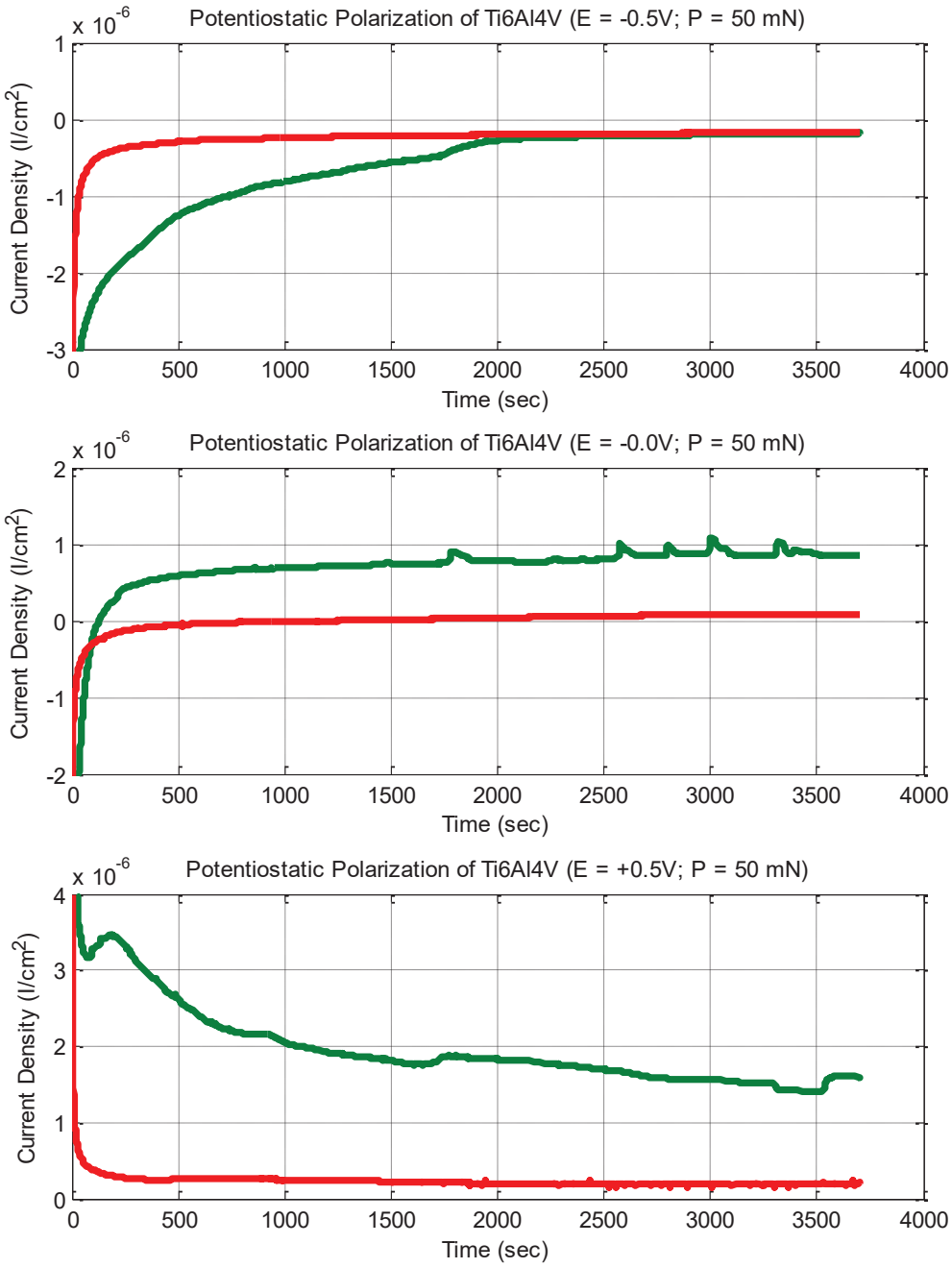

Figure 53: Potentiostatic Polarization of Ti6Al4V with 50 mN of fretting loading

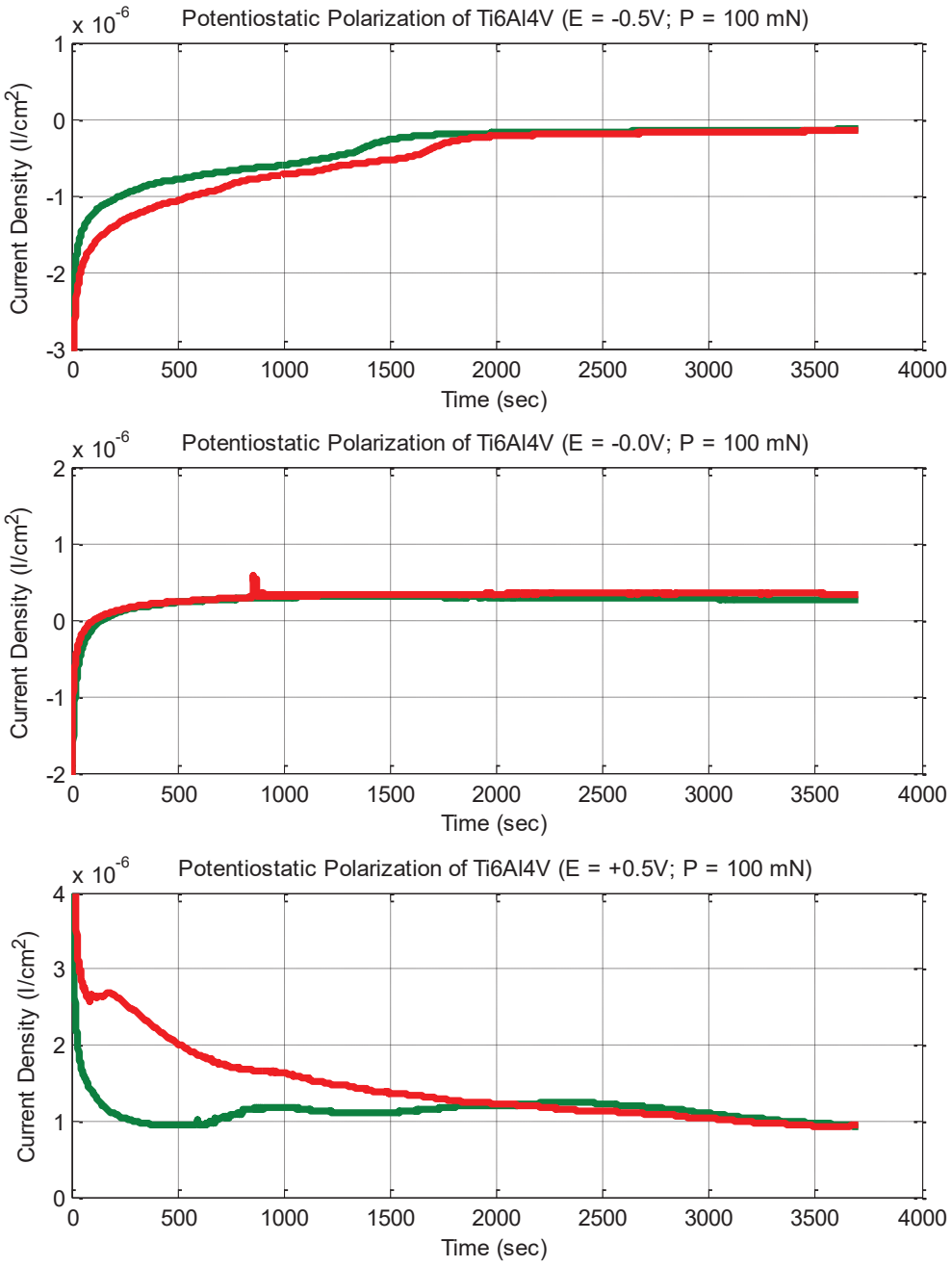

Figure 54: Potentiostatic Polarization of Ti6Al4V with 100 mN of fretting loading

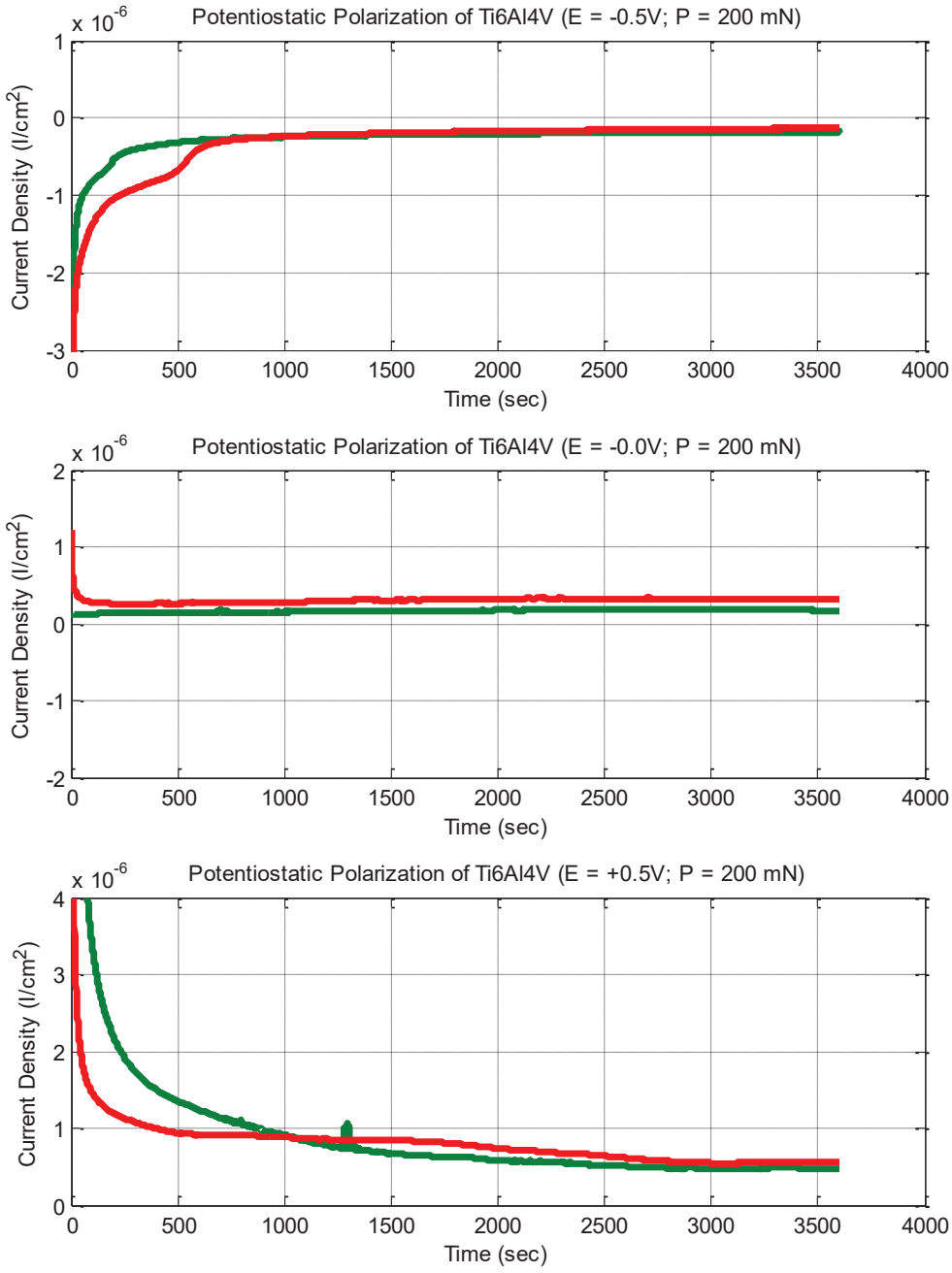

Figure 55: Potentiostatic Polarization of Ti6Al4V with 200 mN of fretting loading

Current density evolution of two surfaces as a function of applied potentials and fretting loads is summarized in Figures 56-57 represents. A statistical representation of Potentiostatic illustrated the active metal dissolution takes place on CoCrMo surface with the increase in both potential and fretting loads while the electrochemical response of Ti6Al4V would be stable in the mechanical and chemical combinations.

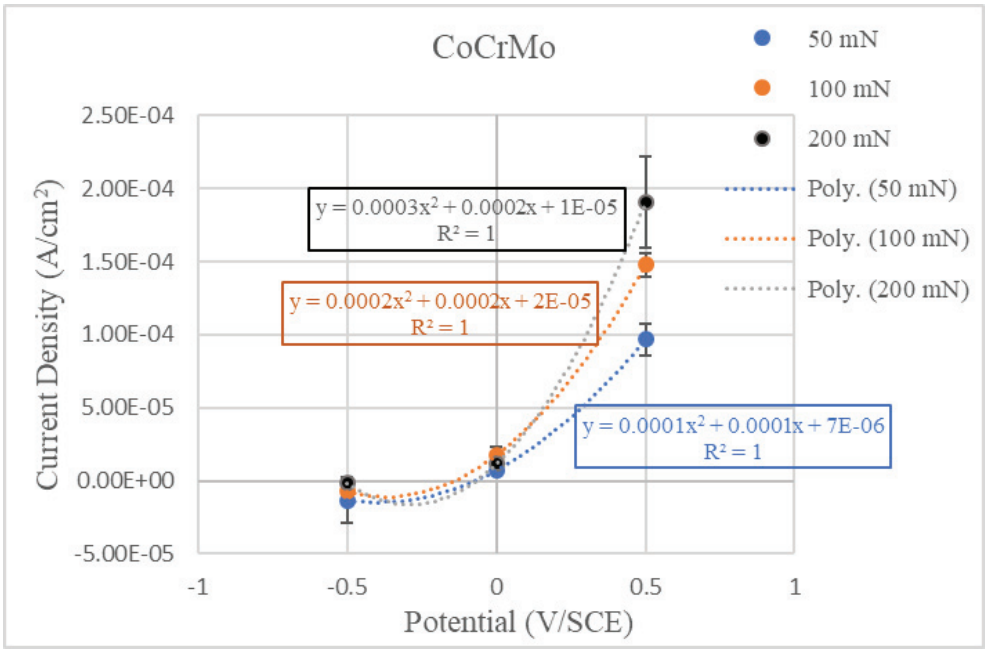

Figure 56: Statistical analysis of Potentiostatic test on CoCrMo

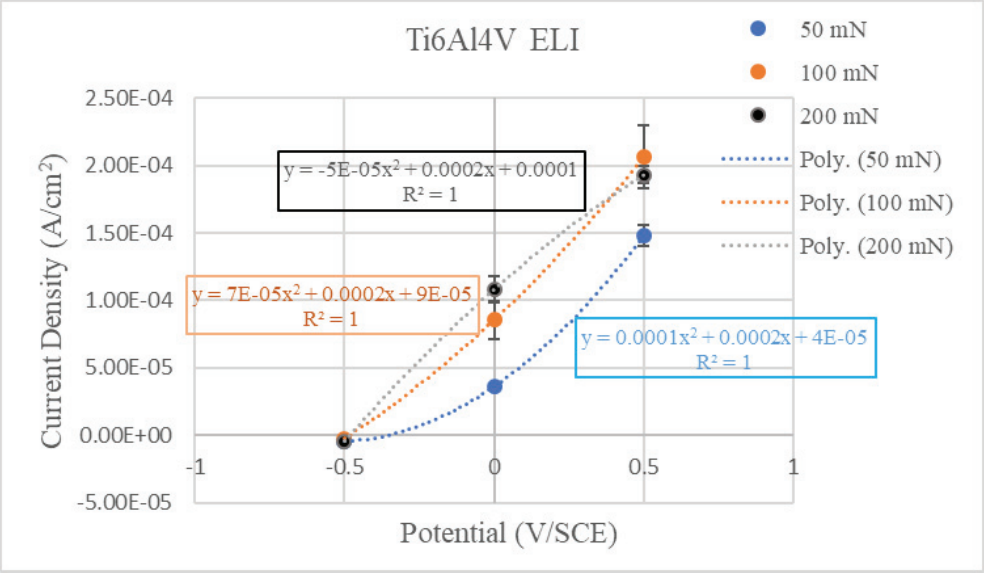

Figure 57: Statistical analysis of Potentiostatic test on Ti6Al4V ELI

Chapter 4: Conclusion

- This study explored the mechanism of corrosion with varying potential. Several important findings where made that have been helpful to understand the behavior of two metals when subjected to three different testings: OCP, PPR, and Potentiostatic Polarization measurement.
- The dwell OCP of Ti6Al4V ELI is low than CoCrMo due to its oxide layer characteristics.
- During fretting, OCP drops more in CoCrMo at all loads than Ti6Al4V ELI suggesting more oxidation on CoCrMo. CoCrMo substrate fretting creates wear debris that is hard that increases further abrasive, adhesive and fatigue wear continuously during fretting. Ti6Al4V ELI substrate fretting creates wear debris that is soft enough to get embedded and remain as a powdered layer on its surface preventing further depletion of metal and thus oxidation. Oxide layer properties showed better results during ball on flat micro motion scratching at 50 mN, 100 m, and 200 mN.
- Relation of COF with the removal of metal at the contacting surface was done. The increase or decrease in COF can be related to drop or rise in potential helping to understand depassivation and repassivation process further.
- After fretting is ceased, CoCrMo reaches its original potential rapidly whereas Ti6Al4V ELI rise in potential was slow and progressive at 100 mN and 200 mN. This though does not suggest that it is corroding at that time. It was observed during Potentiostatic polarization test that even with a high constant voltage applied, it

possesses high current but with no sign of oxidation of depletion of the layer during fretting.

- PPR test result showed a high passive zone for Ti6Al4V ELI. The i_{corr} value is lower by an order of one magnitude suggesting lower corrosion rate. The spontaneous and wide passive zone of it represents less corrosion on higher voltage. CoCrMo was more on an active side and had a transpassive region which represents the dissolution of the metal ion in the electrolyte.
- The potentiostatic test resulted for Ti6Al4V ELI a more stable current at all applied voltage and all loads. CoCrMo exhibited a change in current at 0 and +0.5 V for two loads 100 mN and 200 mN. At 50 mN it was more stable. This suggests that the corrosion rate is higher in CoCrMo than Ti6Al4V ELI.
- Tribocorrosion behavior studied with the above three tests at the operating conditions yielded Ti6Al4V ELI superiority over CoCrMo at varying load.

Chapter 5: Future Work

This thesis helped answer many questions with the understanding of tribocorrosion behavior of CoCrMo and Ti6Al4V ELI. A comparative study was never done before and this was the first effort to explore the biological processes on the corrosion and fretting corrosion behavior of two biomaterials. There remains a series of significant and interesting aspects to be investigated. This research describes several future studies related to the topic. Some part of these studies acts as supporting evidence to the studies done before while some clicks to the new direction. Below is the list of suggestions for future works:

- Total tribological wear long with the parts of individual corrosive and mechanical wear with the wear of synergy can be measured to understand the exact phenomenon. Use of macro-level sample and loads will be helpful and easy to do the test and observe effects from each wear individually and combined.
- These tests were done in a simulated body fluid. The in vivo joint fluid contains more chemicals and proteins. The corrosion behavior of these two metals could be different in that solution. However, it is important to characterize the body fluid in each patient and to find the matching simulating fluid for that.
- The time used for the test was small. The corrosion rate may get affected or get worse in the metal which was good for this test than the other metal. Long term fretting and corrosion study will help understand get more confidence in results obtained.
- The adverse reaction of these metals with the various body cells was not done. It could behave differently in human bodies. Different inflammatory cells can be used to understand the complex behavior of the material with the varying atmosphere.

- The reason for the rise and drop of COF values were visualized and not actually analyzed for the repeatability of nature explained in this thesis. Scratching could be performed at various loads to see the trench and study the depth behavior.
- X-ray Photoelectron spectroscopy can be done to investigate the oxide layer chemistry. It will be also helpful to understand the change in the chemistry of the electrolytic solution used to perform the test. The change in ion concentration will help understand the depassivation process more clearly.
- Use of other tests like Electrochemical Impedance test, Zero-Resistance Ammeter, etc. can be used to study corrosion behavior.

References

[1] "Synovial joint," *Wikipedia*. 29-Dec-2018.

[2] "Synovial fluid," *Wikipedia*. 07-Mar-2019.

[3] "Total Hip Joint Replacement: The Basics You Need to Know," *McLeod Health*, 07-Apr-2015. [Online]. Available: https://www.mcleodhealth.org/blog/total-hip-joint-replacement-basics-need-know/. [Accessed: 20-Nov-2018].

[4] "Hip Replacement Materials - A Complete Guide to the Best and Worst." [Online]. Available: https://www.regenexx.com/blog/research/hip-replacement-materials---a-complete-guide-to-the-best-and-worst/. [Accessed: 20-Nov-2018].

[5] S. Shrestha, "Wear behavior of Ti-6Al-4V for Joint Implants manufactured by Electron Beam Melting," p. 130.

[6] W. Paul, "Table 1: Biomedical Applications of Bioceramics," p. 9.

[7] J. A. López-López *et al.*, "Choice of implant combinations in total hip replacement: systematic review and network meta-analysis," *BMJ*, vol. 359, p. j4651, Nov. 2017.

[8] S. Affatato and L. Grillini, "1 - Topography in bio-tribocorrosion," in *Bio-Tribocorrosion in Biomaterials and Medical Implants*, Y. Yan, Ed. Woodhead Publishing, 2013, pp. 1–22a.

[9] J. Drummond, P. Tran, and C. Fary, "Metal-on-Metal Hip Arthroplasty: A Review of Adverse Reactions and Patient Management," *J. Funct. Biomater.*, vol. 6, no. 3, pp. 486–499, Jun. 2015.

[10] S. Glyn-Jones, H. Pandit, Y.-M. Kwon, H. Doll, H. S. Gill, and D. W. Murray, "Risk factors for inflammatory pseudotumour formation following hip resurfacing," *J. Bone Joint Surg. Br.*, vol. 91-B, no. 12, pp. 1566–1574, Dec. 2009.

[11] D. J. Langton *et al.*, "Adverse reaction to metal debris following hip resurfacing: THE INFLUENCE OF COMPONENT TYPE, ORIENTATION AND VOLUMETRIC WEAR," *J. Bone Joint Surg. Br.*, vol. 93-B, no. 2, pp. 164–171, Feb. 2011.

[12] R. Dattani, "Femoral osteolysis following total hip replacement," *Postgrad. Med. J.*, vol. 83, no. 979, pp. 312–316, May 2007.

[13] R. Narayan, Ed., *Biomedical Materials*. Boston, MA: Springer US, 2009.

[14] J. M. Cuckler, "The Rationale for Metal-on-Metal Total Hip Arthroplasty:," *Clin. Orthop.*, vol. 441, no. NA;, pp. 132–136, Dec. 2005.

[15] N. A. Sandiford, S. K. Muirhead-Allwood, and J. A. Skinner, "Revision of failed hip resurfacing to total hip arthroplasty rapidly relieves pain and improves function in the early post operative period," *J. Orthop. Surg.*, vol. 5, no. 1, p. 88, 2010.

[16] Y. Liao, E. Hoffman, M. Wimmer, A. Fischer, J. Jacobs, and L. Marks, "CoCrMo Metal-on-Metal Hip Replacements," *Phys. Chem. Chem. Phys. PCCP*, vol. 15, no. 3, Jan. 2013.

[17] G. Bellfontaine, "The Corrosion of CoCrMo Alloys for Biomedical Applications," p. 88.

[18] "Cobalt Chrome Molybdenum Bar Stock - Chrome Moly Steel - ASTM F1537 Alloy 1," *United Performance Metals*, 08-Nov-2016. [Online]. Available: https://www.upmet.com/products/cobalt/cobalt-chrome-moly. [Accessed: 21-Nov-2018].

[19] C. Oldani and A. Dominguez, "Titanium as a Biomaterial for Implants," 2012.

[20] "Titanium Specification ASTM F136 | Performance Titanium Group." .

[21] C. Myant, R. Underwood, J. Fan, and P. M. Cann, “Lubrication of metal-on-metal hip joints: The effect of protein content and load on film formation and wear,” *J. Mech. Behav. Biomed. Mater.*, vol. 6, pp. 30–40, Feb. 2012.

[22] R. M. Trommer and M. M. Maru, “Importance of preclinical evaluation of wear in hip implant designs using simulator machines,” *Rev. Bras. Ortop. Engl. Ed.*, vol. 52, no. 3, pp. 251–259, May 2017.

[23] M. A. Wimmer, J. Loos, R. Nassutt, M. Heitkemper, and A. Fischer, “The acting wear mechanisms on metal-on-metal hip joint bearings: in vitro results,” *Wear*, vol. 250, no. 1–12, pp. 129–139, Oct. 2001.

[24] M. Niemczewska-Wójcik, “Wear mechanisms and surface topography of artificial hip joint components at the subsequent stages of tribological tests,” *Measurement*, vol. 107, pp. 89–98, Sep. 2017.

[25] D. Bennett, L. Humphreys, S. O’Brien, C. Kelly, J. Orr, and D. E. Beverland, “The influence of wear paths produced by hip replacement patients during normal walking on wear rates,” *J. Orthop. Res.*, vol. 26, no. 9, pp. 1210–1217, Sep. 2008.

[26] J. Geringer, K. Kim, J. Pellier, and D. D. Macdonald, “3 - Fretting corrosion processes and wear mechanisms in medical implants,” in *Bio-Tribocorrosion in Biomaterials and Medical Implants*, Y. Yan, Ed. Woodhead Publishing, 2013, pp. 45–73.

[27] “AAOS2001-WearinImplants.pdf.” .

[28] “Adhesive Wear - an overview | ScienceDirect Topics.” [Online]. Available: https://www.sciencedirect.com/topics/materials-science/adhesive-wear. [Accessed: 20-Apr-2019].

[29] S. Saroj, C. K. Sahoo, D. Tijo, K. Kumar, and M. Masanta, *Sliding Abrasive Wear Characteristic of TIG Cladded TiC Reinforced Inconel825 Composite Coating*. Elsevier Science Publishers Limited, 2017.

[30] M. Nine, D. Choudhury, A. Hee, R. Mootanah, and N. Osman, "Wear Debris Characterization and Corresponding Biological Response: Artificial Hip and Knee Joints," *Materials*, vol. 7, no. 2, pp. 980–1016, Feb. 2014.

[31] J. Ryu, S. Shrestha, G. Manogharan, and J. Jung, "Sliding Contact Wear Damage of EBM built Ti6Al4V: Influence of Process Induced Anisotropic Microstructure," *Metals*, vol. 8, no. 2, p. 131, Feb. 2018.

[32] J. J. Ryu and P. Shrotriya, "2 - Synergistic mechanisms of bio-tribocorrosion in medical implants," in *Bio-Tribocorrosion in Biomaterials and Medical Implants*, Y. Yan, Ed. Woodhead Publishing, 2013, pp. 25–44.

[33] J. J. Ryu and P. Shrotriya, *Bio-tribocorrosion in biomaterials and medical implants: 2. Synergistic mechanisms of bio-tribocorrosion in medical implants*. Elsevier Inc. Chapters, 2013.

[34] F. Contu, B. Elsener, and H. Böhni, "Corrosion behaviour of CoCrMo implant alloy during fretting in bovine serum," *Corros. Sci.*, vol. 47, no. 8, pp. 1863–1875, Aug. 2005.

[35] B. Sivakumar, S. Kumar, and T. S. N. Sankara Narayanan, "Fretting corrosion behaviour of Ti–6Al–4V alloy in artificial saliva containing varying concentrations of fluoride ions," *Wear*, vol. 270, no. 3–4, pp. 317–324, Jan. 2011.

[36] M. A. Wimmer *et al.*, "Wear mechanisms in metal-on-metal bearings: The importance of tribochemical reaction layers," *J. Orthop. Res.*, p. n/a-n/a, 2009.

[37] S. D. Cook *et al.*, "Wear and corrosion of modular interfaces in total hip replacements," *Clin. Orthop.*, no. 298, pp. 80–88, Jan. 1994.

[38] Y. Liao, E. Hoffman, M. Wimmer, A. Fischer, J. Jacobs, and L. Marks, "CoCrMo metal-on-metal hip replacements," *Phys Chem Chem Phys*, vol. 15, no. 3, pp. 746–756, 2013.

[39] P. Roberge, *Corrosion Engineering : Principles and Practice: Principles and Practice*. Mcgraw-hill, 2008.

[40] B. Alemón, M. Flores, W. Ramírez, J. C. Huegel, and E. Broitman, "Tribocorrosion behavior and ions release of CoCrMo alloy coated with a TiAlVCN/CNx multilayer in simulated body fluid plus bovine serum albumin," *Tribol. Int.*, vol. 81, pp. 159–168, Jan. 2015.

[41] G. Manivasagam, D. Dhinasekaran, and A. Rajamanickam, "Biomedical Implants: Corrosion and its Prevention - A Review~!2009-12-22~!2010-01-20~!2010-05-25~!," *Recent Pat. Corros. Sci.*, vol. 2, no. 1, pp. 40–54, Jun. 2010.

[42] J. J. Jacobs, J. L. Gilbert, and R. M. Urban, "Corrosion of Metal Orthopaedic Implants*:," *J. Bone Joint Surg. Am.*, vol. 80, no. 2, pp. 268–282, Feb. 1998.

[43] P. R. Roberge, *Corrosion Basics: An Introduction*. NACE International, 2006.

[44] D. C. Hansen, "Metal Corrosion in the Human Body: The Ultimate Bio-Corrosion Scenario," *Electrochem. Soc. Interface*, p. 4, 2008.

[45] P. Ponthiaux, F. Wenger, and J.-P. Celis, "Tribocorrosion: Material Behavior Under Combined Conditions of Corrosion and Mechanical Loading," *Corros. Resist.*, p. 28.

[46] L. Benea, E. Dănăilă, P. Ponthiaux, and J.-P. Celis, "Improving tribocorroson behaviour by electro-codeposition of TiC nano-dispersed particles with nickel as hybrid layers for energy applications," *IOP Conf. Ser. Mater. Sci. Eng.*, vol. 174, p. 012045, Feb. 2017.

[47] Satendra Kumar, Sankara Narayanan Tsn, G. S. Raman, and S.K. Seshadri, "Fretting corrosion behaviour of CP-Ti and the implications of using titanium as an implant material." Unpublished, 2009.

[48] Y. Liu and J. L. Gilbert, "The effect of simulated inflammatory conditions and pH on fretting corrosion of CoCrMo alloy surfaces," *Wear*, vol. 390–391, pp. 302–311, Nov. 2017.

[49] S. N. Rosenbloom and R. A. Corbett, "07674 - An Assessment of ASTM F 2129 Electrochemical Testing of Small Medical Implants - Lessons Learned," p. 10.

[50] S. Kumar, B. Sivakumar, T. S. N. Sankara Narayanan, S. Ganesh Sundara Raman, and S. K. Seshadri, "Fretting-corrosion mapping of CP-Ti in Ringer's solution," *Wear*, vol. 268, no. 11–12, pp. 1537–1541, May 2010.

[51] A. Mellado-Valero, A. Muñoz, V. Pina, and M. Sola-Ruiz, "Electrochemical Behaviour and Galvanic Effects of Titanium Implants Coupled to Metallic Suprastructures in Artificial Saliva," *Materials*, vol. 11, no. 1, p. 171, Jan. 2018.

[52] A. Butt *et al.*, "Design, Development, and Testing of a Compact Tribocorrosion Apparatus for Biomedical Applications," *J. Bio- Tribo-Corros.*, vol. 1, no. 1, p. 4, Mar. 2015.